University of Stavanger

Faculty of Science and Technology

BACHELOR`S THESIS

Study program/Specialization: Chemistry and Environmental Engineering/Biological Chemistry and Biotechnology	Spring semester, 2021 Open access
Writers: Lejla Buzaljko and Natalija Jakovljevic	Lejla Buzaljko Natalija Jakovljevic
Faculty supervisor: Emil Lindbäck	
Thesis title: Synthesis of Iminosugar Based Ammonium Compounds as Acetylcholinesterase Inhibitor Candidates – A Potential Strategy for Alzheimer's Treatment	
Credits (ECTS): 20 Points	
Key words: Alzheimer's disease, acetylcholinesterase inhibitors, iminosugars	Pages: 55 (Including Appendix) Stavanger, 31.05.2021

Frontpage for bachelor thesis

Faculty of Science and Technology

Decision made by the Dean October 30th 2009

Abstract

Alzheimer's disease accounts for 60–70% of cases of dementia worldwide, with an estimated global incidence of 50 million cases. Alzheimer's disease is a chronic and fatal illness that causes progressive deterioration of the central nervous system. Cholinergic deficiency is associated with Alzheimer's disease, and various cholinesterase inhibitors have been developed as lead compounds for the treatment of Alzheimer's disease, including naturally derived inhibitors, synthetic analogues and hybrids. Due to the multifactorial nature of Alzheimer's disease, no cure is available for this fatal disease despite huge efforts by the pharmaceutical industry and academia. Indeed, nowadays, the health care system is only able to alleviate the symptoms of Alzheimer's disease patients by providing drugs which belong to the class of drugs called acetylcholinesterase inhibitors.

Through recent studies it has been shown that iminosugars armed with suitable hydrophobic groups behave as very potent acetylcholinesterase inhibitors. Inspired by the very potent acetylcholinesterase inhibitor edrophonium **1** that hosts a permanent positive charge in its ammonium group, in this thesis we aimed to convert an iminosugar into an ammonium compound **11** that also hosts a permanent positive charge on its nitrogen atom. Compound **11** was successfully synthesized in seven steps starting from commercially available L-xylose in an overall total yield of 8%. The synthetic strategy for achieving this was to treat the pyrrolidine **9** with 1,4-dibromobutane and Pd/C catalyzed reduction, which triggered the *N*-spiro cyclization of the iminosugar into a quaternary ammonium salt **11** hosting a positive charge on the nitrogen atom.

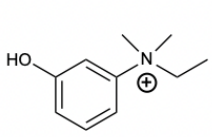

1

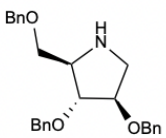

9

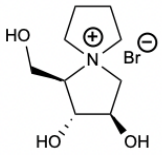

11

Acknowledgements

All work on this thesis was conducted at the University of Stavanger, Department of Chemistry, Bioscience and Environmental Technology, Norway, as part of our Bachelor's degree in Chemistry and Environmental Engineering & Biological Chemistry and Biotechnology. First and foremost, we would like to express our deepest gratitude to Associate Professor Dr. Emil Lindbäck for his professional guidance throughout this project. Emil was always available to answer our questions, and if not in person he would always respond on the telephone or by email, and never failed to give us the necessary guidance and support.

Secondly, we would like to thank PhD student Katja Håheim, for her constant support and guidance throughout this project. Katja always made time to educate us in the laboratory and she even made time to help us during the weekends. During this project we have truly enjoyed working with Katja and we really appreciate her for contributing to a fun and exciting working environment in the laboratory. We would also like to thank PhD student Caroline Vaaland, for sharing her knowledge regarding our project and for being available to help with any practical aspects of our project. Furthermore, thanks to PhD student Vebjørn Eikemo for helping us with naming more complex compounds and Marianne Bore Haarr for taking her time to educate us in the lab. Thanks to Associate Professor Dr. Kåre B. Jøregensen for his help with fixing the NMR spectrometer and the IR apparatus.

Finally, we would like to thank family and friends for their relentless support during our time as bachelor's students and for always encouraging us to do better. During these special times in regard to the global pandemic, they have given us the necessary motivation to always keep going and to work hard.

Selected abbreviations and acronyms

AD – Alzheimer's disease

Aβ – Amyloid beta

Ac - Acetate

ACh – Acetylcholine

AChE – Acetylcholinesterase

AChEI – Acetylcholinesterase inhibitor

BuChE – Butyrylcholinesterase

CAS – Catalytic anionic subsite

ChAT – Choline acetyltransferase

DCM – Dichloromethane

DMF – *N,N*-Dimethylformamide

Et – Ethyl

IR – Infrared

Me – Methyl

NMR – Nuclear magnetic resonance

PAS – Peripheral anionic site

PE – Petroleum ether

RT – Room temperature

TBAF – Tetra-*n*-butylammonium fluoride

T*c*AChE – *Torpedo californica* acetylcholinesterase

THF - Tetrahydrofuran

TLC – Thin-layer chromatography

VAChT – Vesicular acetylcholine transporter

Contents

1 Introduction 7

1.1 Alzheimer's disease 7

1.2 AD's Neuropathology 8

1.3 Cholinergic and Amyloid Hypothesis 9
1.3.1 Cholinesterase and Cholinergic Hypothesis 9
1.3.2 Amyloid Hypothesis 11

1.4 The mechanism of AChE 12

1.5 Traditional AChE Inhibitors 14
1.5.1 Physostigmine 15
1.5.2 Tacrine 15
1.5.2b Synthesis of Tacrine 16
1.5.3 Donepezil 16
1.5.4 Rivastigmine 17
1.5.5 Galantamine 17
1.5.6 Metrifonate 17

1.6 The future of AChE inhibitor 18

1.8 Iminosugars 19

Objectives 20

2 Results and discussion 21
2.1.1 Protection of L-xylose to give the tetra-protected sugar 3 21
2.1.2 Condensation-silyl protection reaction sequence 22
2.1.3 Mesylation protection of compound 5 to yield compound 6 24
2.1.4 Cyclisation to form zwitterion 7 25
2.1.5 Reduction and deoxygenation reaction 26
2.1.6 Formation of the target *N*-spiro fused compound 10 *via* double substitution reaction 27
2.1.7 Benzyl deprotection to furnish target molecule 11 29

2.2 Concluding remarks 30

2.3 Future work 30

3 Experimental 31
3.1 General 31
3.1.1 Solvents and reagents 31
3.1.2 Spectroscopic and spectrometric analysis 31
3.1.3 Chromatography 31

3.2 Methods 32
3.2.1 2,3,5-Tri-*O*-benzyl-L-xylofuranose (3) 32
3.2.2 (2*R*,3*R*,4*S*,*E*)-2,3,5-Tris(benzyloxy)-4-hydroxypentanal *O*-(*tert*-butyldiphenylsilyl) oxime (5) 33
3.2.3 (2*R*,3*R*,4*S*,*E*)-2,3,5-Tris(benzyloxy)-4-metylsulfonyloxypentanal *O*-(*tert*-butyldiphenylsilyl) oxime (6) 34
3.2.4 (2*R*,3*R*,4*R*)-3,4-Bis(benzyloxy)-2-((benzyloxy)methyl)-3,4-dihydro-2*H*-pyrrole 1-oxide (7) 35
3.2.5 (2*R*,3*R*,4*R*)-3,4-Bis(benzyloxy)-2-((benzyloxy)methyl)pyrrolidine (9) 36
3.2.6 (1*R*,2*R*,3*R*)-2,3-Bis(benzyloxy)-1-((benzyloxy)methyl)-5-azaspiro[4.4]nonan-5-ium-bromide (10) 37
3.2.7 (1*R*,2*R*,3*R*)-2,3-Dihydroxy-1-(hydroxymethyl)-5-azaspiro[4.4]nonan-5-ium-bromide (11) 38

4 Appendix 42

4.1 Spectra for compounds 42
4.1.1 2,3,5-Tri-*O*-benzyl-L-xylofuranose (3) 42
4.1.2 (2*R*,3*R*,4*S*, *E*) -2,3,5-Tris(benzyloxy)-4-hydroxypentanal *O*-(*tert*-butyldiphenylsilyl) oxime (5) 44
4.1.3 (2R,3R,4S, E)-2,3,5-Tris(benzyloxy)-4metylsulfonyloxypentanal O-(tert-butyldiphenylsilyl) oxime (6) 46
4.1.4 (2*R*,3*R*,4*R*)-3,4-Bis(benzyloxy)-2-((benzyloxy)methyl)-3,4-dihydro-2*H*-pyrrole 1-oxide (7) 48
4.1.5 (2*R*,3*R*,4*R*)-3,4-Bis(benzyloxy)-2-((benzyloxy)methyl)pyrrolidine (9) 50
4.1.6 (1*R*,2*R*,3*R*) -2,3-Bis(benzyloxy)-1-((benzyloxy)methyl) -5-azaspiro[4.4]nonan-5-ium-bromide (10) 52
4.1.7 (1*R*,2*R*,3*R*)-2,3-Dihydroxy-1-(hydroxymethyl)-5-azaspiro[4.4]nonan-5-ium-bromide (11) 54

1 Introduction

1.1 Alzheimer's disease

Alzheimer's disease (AD) is a neurological disorder named after the German psychiatrists Alois Alzheimer. Amyloid–beta peptide (Aβ) accumulation in the most affected areas of the brain results in formation of neurotic plaques and neurofibrillary tangles. Alois Alzheimer was the first one to notice the presence of amyloid plaques and an extreme loss of neurons while inspecting the brain of patients with AD.[1] The most common symptom of AD is dementia which is characterized by the loss of memory, cognitive functioning and behavioral abilities. In the early stages of the disease the symptoms are just beginning to affect a person's functioning in common daily activities. As the disease progresses to a more severe stage, the person must depend completely on daily caregiving for basic activities of living.[2] Today, the disease is responsible for 60–70% of the senile dementia cases around the globe[3] and it is approximated that it can cause death 3–9 years after a person has been diagnosed with the disease.[4]

At present, it is believed that at least 50 million people are living with AD worldwide and this number is projected to double every 20 years and will reach 152 million by 2050, if no cure is found.[5] The burden of AD affects individuals, their families, and the economy, with estimated global costs of US$ 1 trillion annually.[6] In Norway, the estimated amount of people with dementia is between 80 000–100 000 and the number is estimated to be around 160 000 within the next 30 years.[7] The annual societal costs related to AD in Norway are about 7,46 billion US$ and with the increasing number of Alzheimer's patients the cost will be as high as 14,5 billion US$ in 2040.[8] Needles to mention, as the number of patients suffering from AD is steadily increasing, there is going to be a challenge for the society to provide healthcare for all patients. For obvious reasons, there is an urgent need to develop drugs that can reverse or at least freeze the progression of AD.[9]

1.2 AD's Neuropathology

The first known description of Alzheimer's dates back to 1907.[10] Now, more than 100 years later and despite enormous effort and investments, there is still no cure developed for this fatal disease. The exact causative effects of Alzheimer's are not fully understood,[11] however, factors that seem to play an essential role in the development of the disease are neuron loss, extracellular β-amyloid deposits, τ-protein hyperphosphorylation, and neurotransmitter system dysfunction.[12] Other factors, including age (which is the strongest trigger for developing the disease),[13] education, genetic aspect and dental health are among the expected factors to be involved in the progression of Alzheimer's.[14] In addition, studies indicate that maintaining strong social connections and mental activity (neurological stimulation) lower the risk of cognitive decline and further Alzheimer's. This may be due to the direct mechanism through which social and mental stimulation strengthen connections between nerve cells in the brain.[15] While age increases the risk of developing the disease, it is not a direct cause of Alzheimer's. Most individuals with the disease are 65 or older, after which, the risk of Alzheimer's doubles every five years. After the age of 85, the risk reaches nearly one-third. Another strong risk factor for AD is genetics. Those who have family members that have been affected by Alzheimer's are more likely to develop the disease.[16] Because of the multifactorial ethology of the disease and that the exact causative effects have not been sorted, no cure for Alzheimer's disease has been developed.[11]

1.3 Cholinergic and Amyloid Hypothesis

AD has for most of its time and to this day been considered a multifactorial disease, associated with several risk factors as mentioned previously. The underlying cause of the pathological changes in AD is still not discovered, but several hypotheses have been proposed for its cause. It is believed that an impairment in the cholinergic function and an alteration in amyloid β-protein production initiate the disease. These two suggestions have led to the two main hypothesis for AD; the cholinergic hypothesis and the amyloid hypothesis.[1]

1.3.1 Cholinesterases and Cholinergic Hypothesis

Acetylcholinesterase (AChE) and butyrylcholinesterase (BuChE) are enzymes which belong to the group of cholinesterases. AChE catalyzes the hydrolysis of the neurotransmitter acetylcholine (ACh) into acetic acid and choline (*Scheme 1*) and is one of the most crucial enzymes for nerve response.[17] AChE is mainly associated with nerves and muscles, typically being found on the synapsies, while BuChE, also known as plasma cholinesterase, hydrolyses butyrylcholinesterase and is synthesized by the liver.

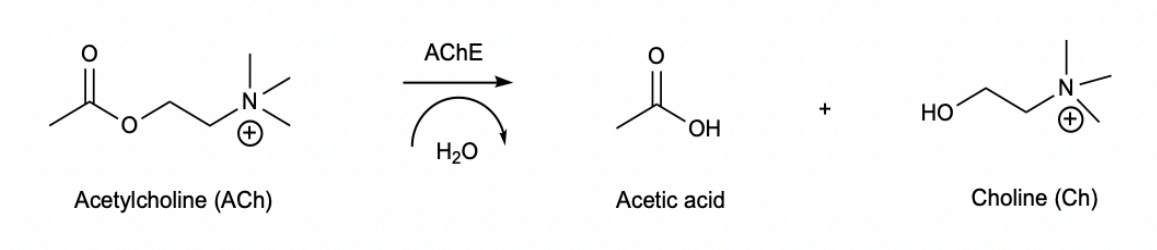

Scheme 1. Acetylcholinesterase hydrolyzes acetylcholine into acetic acid and choline.

In the 1970s, it was believed that cholinergic deficits were related to the enzyme, choline acetyltransferase (ChAT)[1], which is responsible for the synthesis of ACh. The cholinergic hypothesis of AD was proposed due to the critical role of ACh in cognitive functioning. The ACh-synthesis takes place in the cytoplasm of cholinergic neurons. ACh is synthesized from choline and acetyl-coenzyme A by the ChAT enzyme and transported to the synaptic vesicles by vesicular acetylcholine transporter (VAChT).

In the brain, ACh has a crucial role in several physiological processes such as memory, attention, learning and other critical cognitive functions. According to the cholinergic hypothesis, AD is due to the reduction in ACh biosynthesis. Increasing the cholinergic levels by inhibiting AChE is considered to be one of the therapeutic strategies that can promote cognitive and neural cell function. Acetylcholinesterase inhibitors (AChEIs) are used to inhibit ACh degradation in the synapses, which results in continuous accumulation of ACh and activation of cholinergic receptors.[1]

Inhibition of acetylcholinesterase is the most common approach to enhance the well-being of patients with mild to moderate AD. These drugs increase the duration of ACh in the cholinergic synapse, by inhibiting the AChE enzyme from breaking down the neurotransmitter acetylcholine. Such AD treatment is in line with the cholinergic hypothesis, which was presented over 40 years ago.[18] This premise has since then served as the basis for the majority of treatment strategies and drug development approaches for Alzheimer's disease. Aβ is believed to affect cholinergic neurotransmission and to cause a reduction in the choline uptake and release of ACh. It has been demonstrated that a loss on the cholinergic synapses and amyloid fibril formation are related to the neurotoxicity of Aβ oligomers and with the interactions between AChE and Aβ peptide.

As a result, the cholinergic hypothesis is based on three concepts: (1) reduced presynaptic cholinergic markers in the cerebral cortex, (2) severe neurodegeneration of nucleus basalis of Meynert (NMB) in the basal forebrain, which is the source of cortical cholinergic innervation, (3) and the role of cholinergic antagonists in memory decline compared to the agonists, which have the opposite effect.[1, 19] However, recent studies of the brain of patients who had mild cognitive impairment in the early stages of Alzheimer's disease in which acetylcholinesterase activity was unaffected (or even up regulated) have, however, led some to challenge the validity of the hypothesis as well as the rationale for using cholinesterase inhibitors to treat the disorder, particularly in the earlier stages.[20]

1.3.2 Amyloid Hypothesis

For decades, it has been recognized that abnormal deposition of β-sheets in the central nervous system has had a strong interference with dementia, and this has led to the concept of the amyloid hypothesis.[21] The amyloid hypothesis offers a robust framework to explain the Aβ mediated pathogenesis in AD and has for a long time been associated with the disease. According to the hypothesis, accumulation of Aβ peptides in the hippocampus and entorhinal cortex is the driving force behind the AD pathogenesis.[21] The deposition of Aβ peptides can then lead to the decline in the cognitive abilities in AD patients.[21] It is believed that the accumulation of Aβ starts around 15–20 years before the appearance of any observable clinical symptoms.[21] Studies suggested that numerous types of Aβ aggregates, ranging from oligomers to fibrils, contributing to the progression of AD.[21]

Nonetheless, the exact mechanisms of toxicity of Aβ oligomers are still under debate. Aβ oligomers bind to the plasma membranes of neurons and weaken the neuronal function by inducing synaptic dysfunction and mitochondrial dysregulation.[21] They can also activate glutamatergic synaptic transmission, oxidative stress, calcium dyshomeostasis, and inflammation which further contribute to the death and damage of brain cells.[21] All these reports suggest critical involvement of Aβ in AD progression and thus enormous effort has been directed towards stopping the formation of Aβ plaques. Either targeting Aβ alone or the macromolecules involved in the accumulation of Aβ remain promising treatment strategies for controlling AD.[21]

1.4 The mechanism of AChE

The principal role of AChE is the termination of transmission at the cholinergic synapses by rapid hydrolysis of the neurotransmitter ACh. Due to the crucial biological role of AChE, it has become the target of the first generation of anti-Alzheimer drugs.[22]

X-ray analysis of the *Torpedo californica* acetylcholinesterase (*Tc*AChE) revealed a catalytic triad nearby the bottom of a ~ 20 Å deep active gorge decorated with aromatic residues penetrating almost halfway into the enzyme.[23] The residues are highly conserved, and most of them can be assigned functional roles. Trp84 (Trp=tryptophane) and F330 (F=phenylaniline) are involved in the anionic- and esteratic subsite (AS and ES) of the catalytic site (CAS) establishing cation-π interactions with the quaternary ammonium group of the enzyme substrate. Therefore, these interactions stabilize the enzyme-substrate complex and are in general very important in biological systems. On the mouth of the gorge, there is a second binding site termed the peripheral anionic site (PAS). The PAS serves as a relay station for the substrate to the active site. Crystallographic studies have demonstrated the involvement of several of these conserved aromatic residues in interactions with acetylcholinesterase inhibitors via noncovalent interactions.[22] One such example is found in the complex between AChE and edrophonium (**1**) that is a very potent AChE inhibitor in which the quaternary ammonium group of the inhibitor establishes a cation-π interaction with a tryptophan residue in the CAS whereas the hydroxyl group in edrophonium participates in a hydrogen bond with the serin residue in the catalytic triad (*Figure 1*).

The PAS plays a non-cholinergic function in the progress of AD as it has been found to promote the aggregation of Aβ protein into amyloid fibrils, which is involved in the formation of senile plaques.[24] In line with this observation, it has been found that AChEIs that bind exclusively to the PAS inhibit AChE promoted Aβ aggregation.[24] In addition, dual binding site AChEIs (i.e., inhibitors that bind simultaneously to the PAS and the CAS) have been found not only to inhibit the hydrolysis of ACh but also AChE promoted aggregation of Aβ protein,[24] which are both attractive targets for AD treatment.[24] Therefore the design of new types of inhibitors of AChE should be based on the hypothesis of the dual binding of AChE inhibitors.[17]

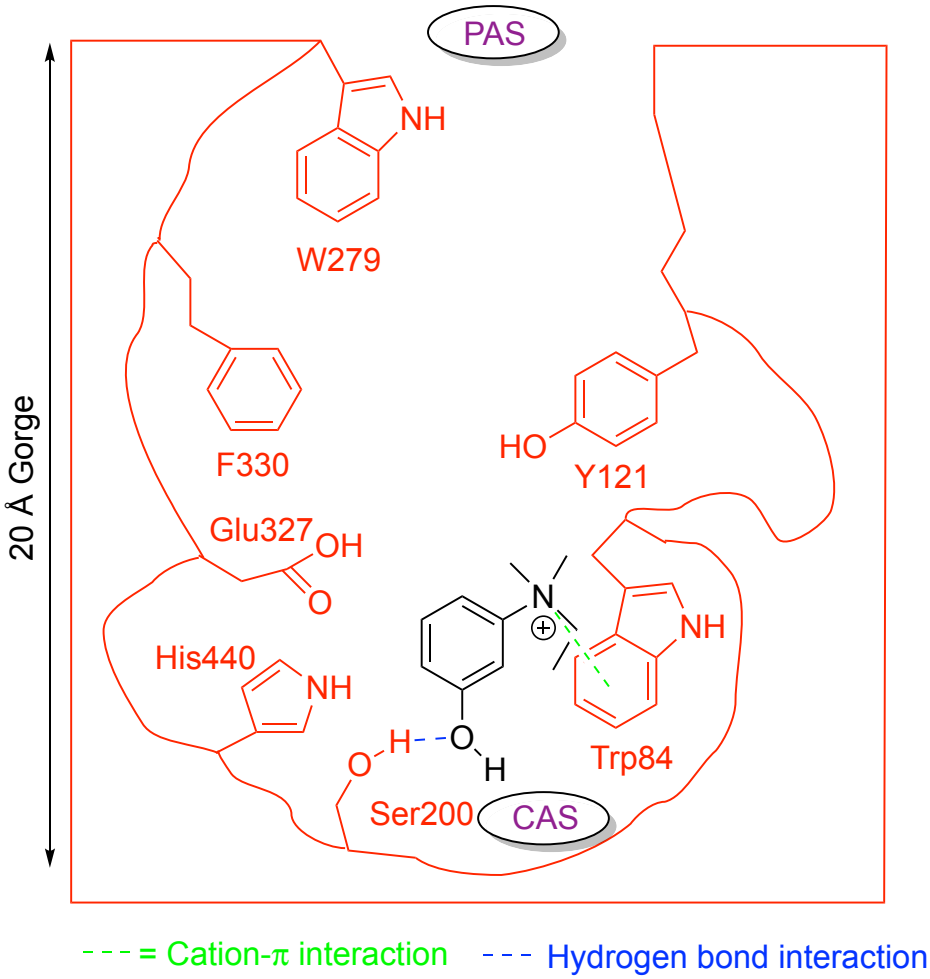

*Figure 1. The active site of AChE interacts with edrophonium (**1**) by cation-π interactions with a tryptophan residue in the CAS whereas the hydroxyl group participates in a hydrogen bond with the serine residue.*

1.5 Traditional AChE Inhibitors

The elucidation and characterization of the pathophysiology of AD suggests a plethora of targets for designing potential disease-modifying agents. These agents should, by definition, be able to alter the underlying pathophysiology of the disease and to demonstrate meaningful reduction in the rate of cognitive decline or in the progression of the disorder.[25] Three general disease-modifying approaches have been acknowledged for the treatment of AD; anti-amyloid, neuroprotective, and restorative. Thus far, three AChE inhibitors have been approved by the Food and Drug Administration (FDA) for the treatment of AD, which include donepezil (**C**), galantamine (**E**) and rivastigmine (**D**) (*Figure 2*).[3, 25] The most traditional inhibitors will be examined in greater detail in the following sections.

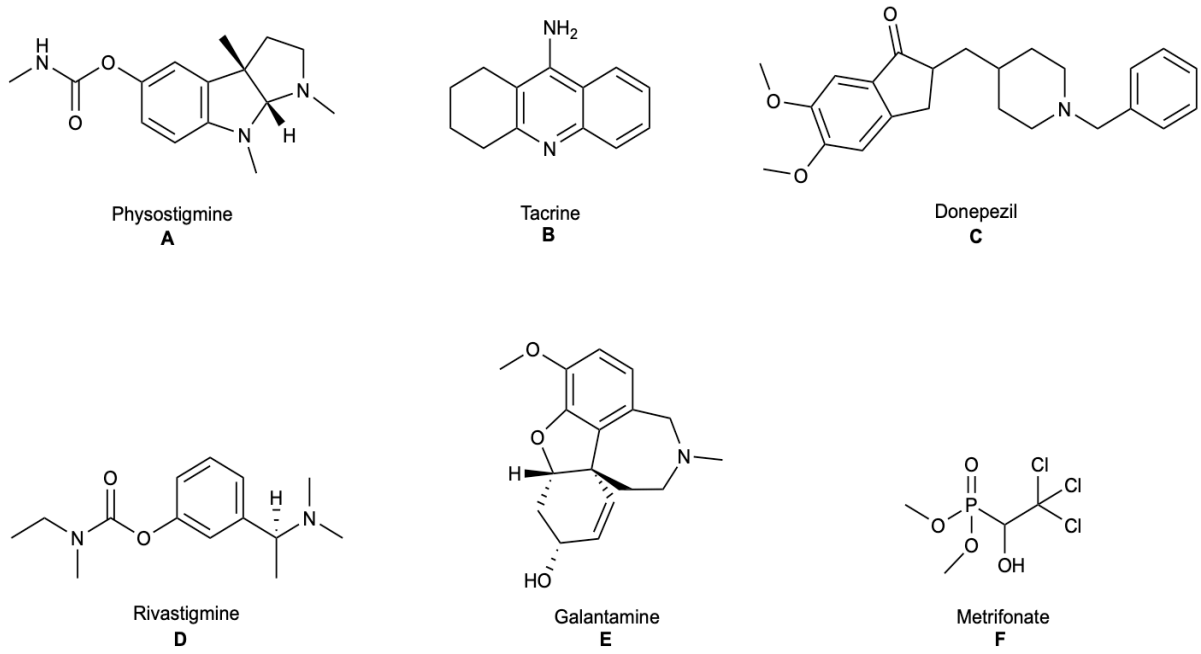

Figure 2. Chemical structures of some traditional AChE inhibitors.

1.5.1 Physostigmine

Eserine, also known as physostigmine (**A)**, that is a potent AChE inhibitor, was first isolated from Calabar beans in 1864. Physostigmine can cross the blood-brain barrier (BBB), but due to the short half-life time, this drug only has a narrow therapeutic index and presents various side effects. Its common side effects include diarrhea, stomach cramps, increased production of saliva and excessive sweating.[3] Due to these disadvantages, physostigmine failed in the clinical trials for the treatment of AD.

1.5.2 Tacrine

Tacrine (**B)**, 9-amino-1,2,3-tetrahydroacridine, was first synthesized in the 1930s, and is a mixed AChE and BuChE inhibitor. Tacrine was originally used as a muscle relaxant antagonists and respiratory stimulant[3] before Heilbronn described the effect tacrine exhibits on AChE and BuChE in 1961. She demonstrated that the compound acts as a reversible inhibitor being partly competitive with the substrate ACh and a more than 1000 times more potent inhibitor of BuChE than of AChE.[17] Other than being and enzyme inhibitor, tacrine (**B**) was found to have other mechanisms which could explain the cholinergic effect. In electrophysiological studies with neurons of *Lymnaea stagnali,* tacrine inhibits a slow outward K^+ current and consequently increases the duration of the action potentials. An action potential is a frequent sequence of changes in the voltage across a membrane which is determined at any time by the relative ratio of ions and the permeability of each ion.[26] Tacrine has been used for the treatment of patient with AD since the 1980s, and was approved by the Food and drug Administration (FDA) in 1993 and then discontinued in 2013. The usage of tacrine is limited due to its many side effects, including nausea, vomiting, loss of appetite, diarrhea and clumsiness affecting a significant number of the patients.[3] Additionally, multiple-dosage regimens are required to maintain prolonged therapeutic activity, due to the short half-life of tacrine.[3] Tacrine interacts with the amino acid residues F330 and Trp84, which are present in the AS and ES of AChE and its molecular structure, **B**, is presented in *Figure 2*.[3]

1.5.2b Synthesis of Tacrine

The Friedländer reaction is an important approach to the synthesis of Tacrine (*Scheme 2*).[27] The Friedländer reaction is a well–known method for preparing quinolines and related bicyclic aza-aromatic compounds.[27] In its original form, the Friedländer reaction is the reaction between an *ortho*-aminobenzaldehyde and an aldehyde or ketone bearing α–methylene functionality. In this regard, condensation reactions between 2-aminobenzonitrile and cyclohexanone, have been recognized as an important and general approach to the synthesis of tacrine and its analogues. This reaction is performed in the presence of a Lewis acid, such as $AlCl_3$, $ZnCl_2$ or $CuCl_2$, under solvent free conditions.[27]

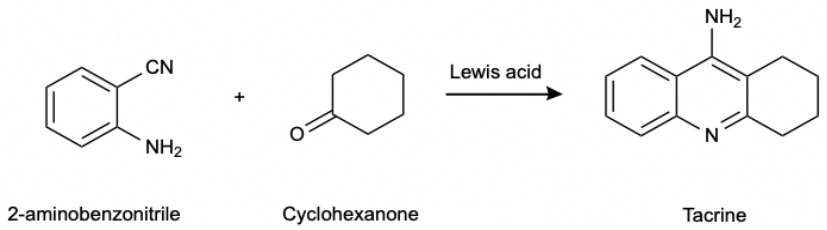

Scheme 2. Synthesis of tacrine from 2-aminobenzonitrile and cyclohexanone in the presence of a Lewis acid.

1.5.3 Donepezil

In 1996, the drug donepezil (**C**), sold under the trade name Aricept (*Figure 2*), was approved by the FDA for the treatment of mild to moderate AD. However, donepezil has presented various side effects, including insomnia, nausea, loss of appetite, diarrhea, muscle cramps and muscle weakness.[28] In addition to inhibit AChE, donepezil may have additional mechanisms of action that exceeds the neurotransmitter level. For instance it also acts at the molecular and cellular level in almost all stages involved in the pathogenesis of AD.[3] Donepezil (**C**) exhibits a unique molecular structure (illustrated in *Figure 2*) that causes simultaneous interactions with CAS and PAS in the active gorge of AChE.[3]

1.5.4 Rivastigmine

Rivastigmine (**D**), sold under the trade name Exelon (*Figure 2*), was approved for the treatment of mild to moderate AD in 2000.[3] Although the exact mechanism of action of rivastigmine is uncertain, it has been hypothesized that it may exert pharmacological action by increasing the cholinergic functions.[3] Rivastigmine is a dual AChE-BuChE inhibitor and it is a carbamate that binds to AChE, which cleaves rivastigmine into various phenolic derivatives that are rapidly excreted from the body.[3] The carbamate moiety binds to the ES of AChE with more affinity than that of the acetate moiety of ACh during ACh hydrolysis. Therefore, the enzyme is inactivated for a certain amount of time[3], offering an explanation to its unusually slow activation kinetics.[3] Rivastigmine has major side effects, including stomach pain, weight loss, diarrhea, loss of appetite, nausea and vomiting.[3]

1.5.5 Galantamine

Galantamine (**E**), marketed with the name Nivalin, is an alkaloid isolated from the *Galanthus woronowij* plant that has been used as a medicine in Eastern European countries for decades for the treatment of myopathy, myasthenia, and sensory and motor deficits associated with the CNS.[3] Galantamine has also been shown to bind to nicotinic cholinergic receptors and its activity against ChE was first identified in the 1950s.[3] Galantamine was approved for the treatment of AD in 2001.[3] Galantamine has since then shown to be effective in treating the cognitive symptoms of AD.[3] The main side effects of galantamine include severe nausea, stomach cramps, vomiting, irregular breathing, confusion, muscle weakness and watering eyes.[3] The chemical structure of galantamine (**E**) is presented in *Figure 2.*

1.5.6 Metrifonate

Metrifonate (**F**) (*Figure* 2) is a organophosphate AChE inhibitor.[3] Metrifonate can improve cholinergic neurotransmission via a pharmacologically active metabolite, 2,2-dichlorovinyl dimethyl phosphate, and has been tested for the treatment of AD.[3] Metrifonate administered once per day can improve the cognitive function of patients with mild to moderate AD.[3] The tolerability of metrifonate is good, but its long-term use causes adverse side effects, including problems with neuromuscular transmission and respiratory paralysis.[3] Therefore, the development of this drug was interrupted during Phase III of clinical trials.[3]

1.6 The future of AChE inhibitor

Since the discovery of the first AChE inhibitor, physostigmine, a large number of studies have been performed to identify more effective inhibitors. Traditional inhibitors are naturally derived agents, other inhibitors may include analogues of the traditional inhibitors, derivatives of natural compounds and hybrids of synthetic inhibitors. The future AChE inhibitors may cause milder side effects than traditional ones and may have better BBB permeability and increased effectiveness.[3] In addition, these compounds are able to limit the progression of AD. Huge efforts have been made in the investigation of AChE inhibition,[3] but only a few drugs have been tested in humans, such as the above-mentioned tacrine (**B**), donepezil (**C**) rivastigmine (**D**) and galantamine (**E**). Most of these inhibitors have only been scarcely studied in animal models or using *in vitro* and *in silico* models. For that reason, further studies in humans are required in order to investigate the safety, efficacy and toxicity of these drugs.[3]

AChE inhibitors are not able to completely stop the progression of AD, and various single-target drugs that have reached clinical trials were not able to effectively alter the state of patients with AD. Therefore, there is a need to develop multi-functional drugs that can target several of the pathological mechanisms involved in the progression of AD, including the decreased levels of ACh, protein misfolding and associated Aβ aggregation, hyperphosphorylation of τ protein, metal dyshomeostasis and oxidative stress. However, there has only been done a limited number of studies that have focused on the development of new multi-target drugs. According to the structure-activity relationship studies, the design of future novel potent multi-target inhibitors should contain the following characteristics;[3] 1) the presence of a positively charged nitrogen atom 2) the size of an alkyl chain that is attached to the nitrogen atom should be relatively small, such as a methyl group; 3) the presence of an oxygen atom that is able to form hydrogen bonds, such as an ester; 4) the presence of electron-donating groups such as hydroxyl groups; and 5) the presence of a two-carbon unit between the nitrogen and oxygen atoms. Especially, the size of the molecule should be small, since large molecules can exhibit decreased activity.[3]

1.8 Iminosugars

Iminosugars (**G-J** in *Figure 3*) are nitrogen-in-ring monosaccharide analogues in which the ring-oxygen atom is replaced by a nitrogen atom. Azasugars (**K** in *Figure 3)* are a similar type of monosaccharide mimetics that contain a nitrogen atom in place of a carbon atom.[29] The most important role of azasugars and iminosugars is their inhibitory potency of glycosidase, which is a result of their ability to be protonated at physiological pH (pH 7,4) and thereby resemble charged analogues of the transition state for enzymatic cleavage of glycosides. Because of their unique ability to inhibit the activity of glycosidases, aza- and iminosugars have been evaluated for the treatment of disorders such as diabetes, cancer, viral infections, and lysosomal storage disorders.[24]

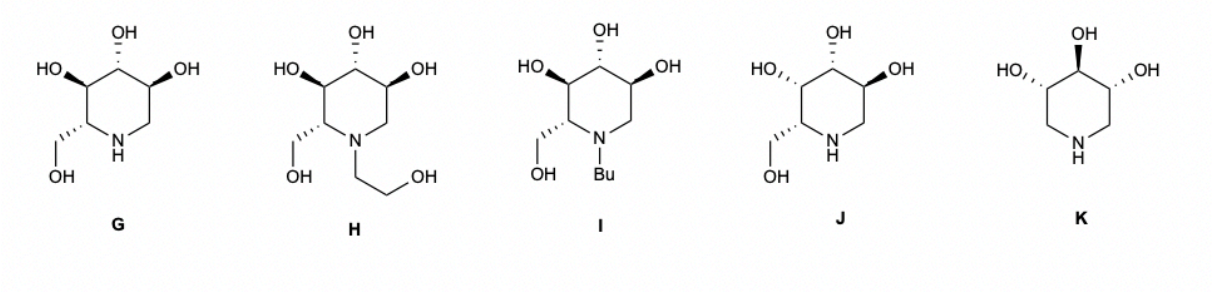

*Figure 3. Structure of iminosugars (**G-J**) and azasugar (**K**).*

The biological activity of iminosugars goes beyond the inhibition of glycosidases. For instance, it has been found that some iminosugars behave as potent inhibitors of acetylcholinesterase, thereby increasing both the level and duration of acetylcholine in the central nervous system. It has been proposed that iminosugars in their protonated form, at least to some extent, resemble the charged substrate of ACh, which is an important aspect for generating interactions with the active gorge of AChE.[24]

Objectives

The goal of this BSc project was to install a permanent positive charge on the nitrogen atom of an iminosugar to obtain compound **11**, which represents an acetylcholinesterase inhibitor candidate. We argued that the positive charge in compound **11** has the potential to establish cation-π interaction with the aromatic residues in the active gorge of AChE (*Figure 4*) in a similar way as edrophonium (**1**) (*Figure 1*). In addition, the hydroxyl groups in compound **11** have the potential to establish hydrogen bonds with the residues in the active gorge of AChE and thus further strengthen the binding to AChE.

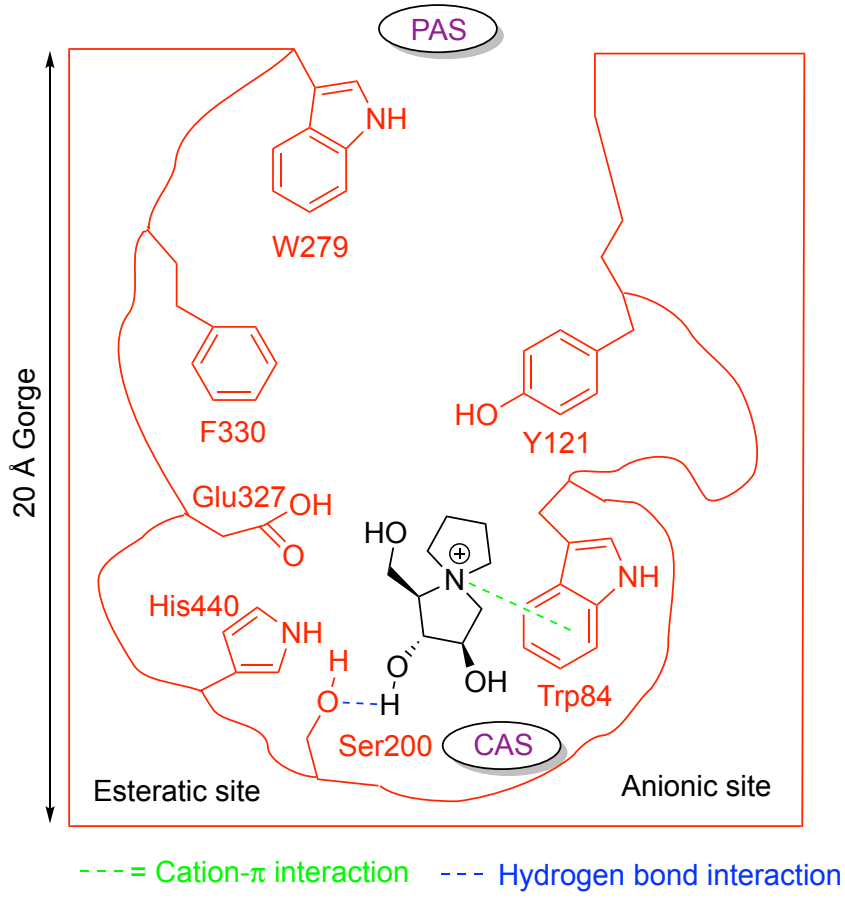

*Figure 4. The active site of AChE interacts with Target molecule (**11**) by cation-π interactions with a tryptophan residue in the CAS whereas the hydroxyl group participates in a hydrogen bond with the serine residue of the catalytic traid.*

2 Results and discussion

2.1.1 Protection of L-xylose to give the tetra-protected sugar 3

In this thesis, the starting material of the synthetic pathway was L-xylose. In order to avoid unwanted reactions occurring on the highly reactive hydroxyl groups of the sugar, the starting material was subjected to a three-step procedure to protect its *hydroxyl* groups in the 2, 3, and 5 positions. Firstly, the most reactive *hydroxyl* group, namely the one at the anomeric carbon was methyl-protected using the traditional Fischer glycosylation conditions; consisting of an acid catalyzed reaction between L-xylose and methanol to give the corresponding methyl-glycoside (*Scheme 3*).[30] The mechanism is initiated by protonation of the hydroxyl group, followed by the elimination of a water molecule, leading to the formation of a resonance stabilized carbocation intermediate **II** (*Scheme 3*). The lone pair electrons of the alcohol then attack the newly formed carbocation, forming an oxonium ion **III**, from which a proton is then eliminated by electron rearrangement to give the desired methyl-glycoside **1** (*Scheme 3*).

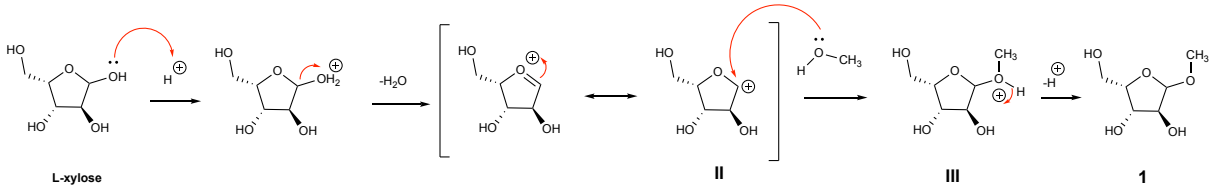

*Scheme 3. Mechanism of Fischer–Helferich glycosylation of L-xylose to give the protected sugar **1**.*

In the subsequent step, methyl glycoside **1** underwent global *O*-benzylation upon treatment with benzyl bromide in the presence of NaH in DMF to provide compound **2** (*Scheme 4*). Benzyl protection is preferably used over other protecting groups such as acetyl i.e., due to their ease to install, in addition they can be easily removed under mild reaction conditions.[31] Finally, the anomeric hydroxyl group of compound **2** was liberated upon treatment with HCl(aq) at elevated temperature to provide furanose **3** in 46% yield over three steps with only one purification (*Scheme 4*).

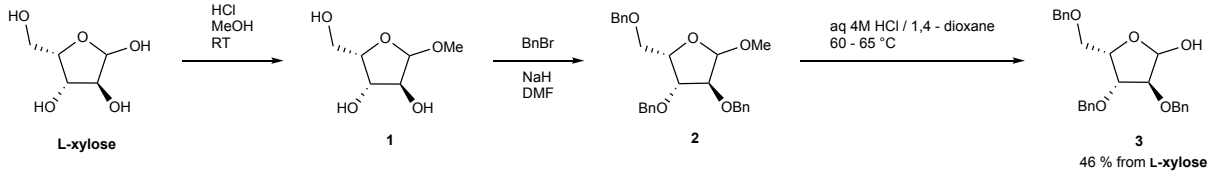

*Scheme 4. Transformation of L-xylose into its corresponding benzyl protected glycoside **3***

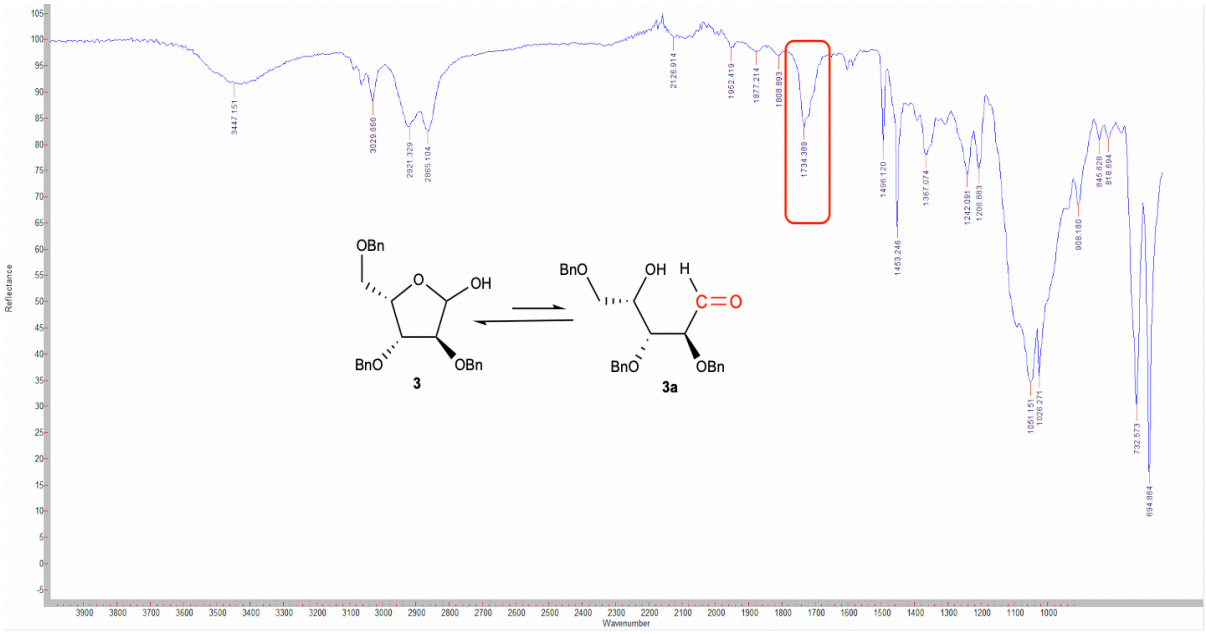

*Figure 5. IR spectra showing that compound **3** exists in equilibrium with its cyclic and acyclic form.*

Upon obtaining the IR spectra of compound **3**, evidence of the equilibrium between the cyclic **3** and acyclic form **3a** could be observed (*Figure 5*). The presence of a low-intensity C=O peak at 1734 cm^{-1} indicates the presence of the aldehyde functionality (highlighted in red color in *Figure* 5) in acyclic compound **3a** (*Figure 5*).

2.1.2 Condensation-silyl protection reaction sequence

This reaction was performed with the motivation to incorporate a nitrogen nucleus into the sugar moiety for the target molecule and to silyl-protect the formed hydroxylamine. Silyl-protection was performed to allow functionalization of the hydroxyl group in the 4-position (*Scheme 5*).

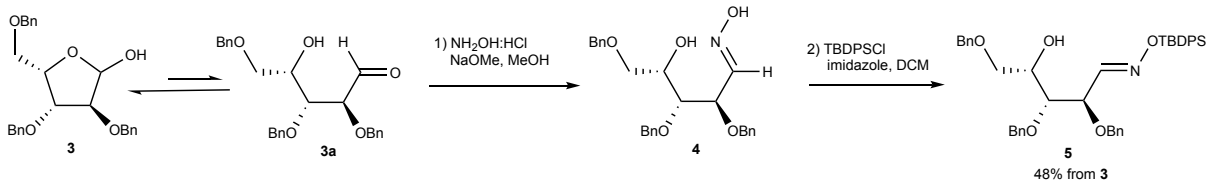

*Scheme 5. The equilibrium mixture of compound **3** undergoing incorporation of a nitrogen nucleus and silyl-protection to form hydroxylamine **5**.*

Thus, when the equilibrium mixture of **3** and **3a** is treated with hydroxylamine (generated *in situ* from hydroxylammonium chloride and sodium methoxide), it is likely that the equilibrium is forced towards aldehyde **3a** according to the Le Châtelier's principle when it reacts with the NH_2OH-nucleophile to generate aldoxime **4** (*Scheme 6*).

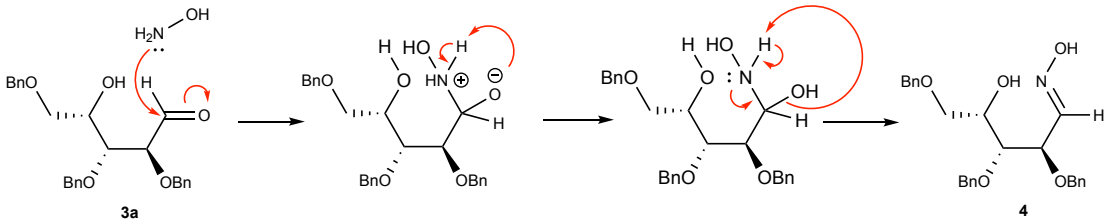

Scheme 6. Mechanism of the incorporation of nitrogen into the sugar moiety

The formation of aldoxime **4** is initiated by a nucleophilic attack of NH_2OH on the carbonyl carbon of **3a** generating a tetrahedral intermediate from which water is eliminated to give aldoxime **4** (*Scheme 6*).

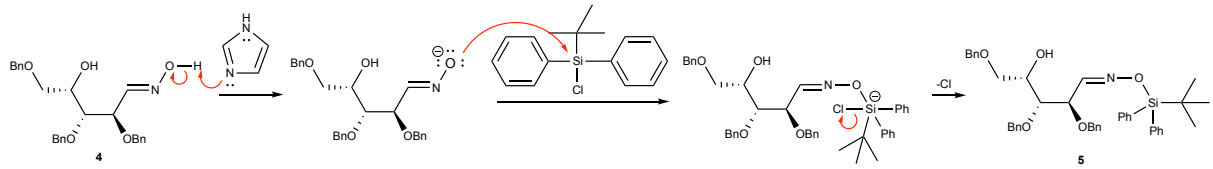

*Scheme 7. Mechanism of the silyl-protection of compound **5**.*

In the following step, oxime **4** underwent selective *O*-silylation on the oxime functionality with *tert*-butyldiphenylsilyl chloride (TBDPSCl) promoted by imidazole to afford silylether **5** in 48% yield over two steps from **3** (*Scheme 7.*). Imidazole acts as a base for the deprotonation of **4** leaving the oxygen with lone pair electrons, initiating a nucleophilic attack onto the silyl group, yielding silyl protected aldoxime **5** upon the expulsion of Cl as a leaving group (*Scheme 7*).

2.1.3 Mesylation protection of compound 5 to yield compound 6

Hydroxyl groups act as bad leaving groups because of their strong basic characteristics and must therefore be converted into better leaving groups. A classical way to convert a hydroxyl group to a good leaving group is to convert it into mesylates.[32] Following this line, alcohol **5** was converted into mesylate **6** in 73-86% yield upon treatment with mesyl chloride in the presence of Et_3N. This reaction was performed with the sole purpose to facilitate a good leaving group for the ring closure onto C-4 (*Scheme 8*).

Scheme 8. O-mesylation of hydroxide to yield the mesyl-protected ***6****.*

The base deprotonates the hydrogen on the mesyl chloride allowing for electron donation and integration of a negative charge on the carbon atom (*Scheme 9*). The lone pair electrons on the carbon then attack the sulfur atom which further breaks the sulfur-oxygen bond, generating a negative charge on the oxygen. The electron on the oxygen then forms a new double bond between sulfur and further expels Cl. Finally, the lone pair electrons on the hydroxide of compound **5** attack the sulfur and by electron transfer providing compound **6** in 87% yield (*Scheme 9*).

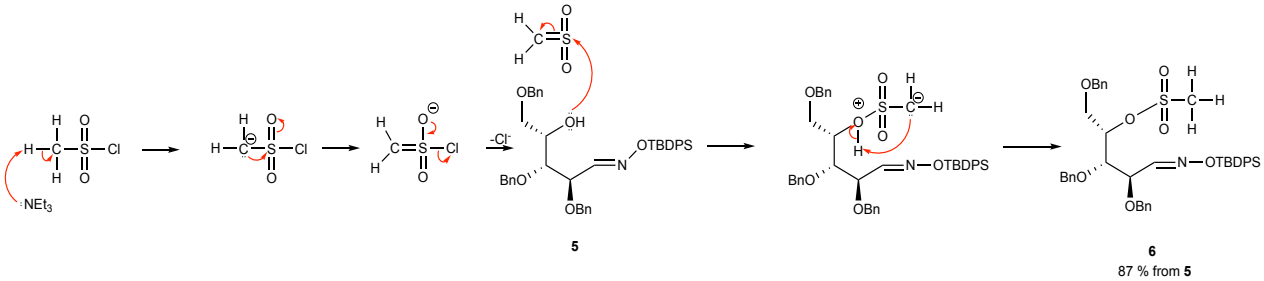

Scheme 9. Mechanism of the O-mesylation of compound ***5*** *to yield the mesyl-protected* ***6****.*

2.1.4 Cyclisation to form zwitterion 7

In this step of the synthesis, the silyl-protecting group was removed with the purpose to trigger the cyclisation of compound **6** into compound **7** (*Scheme 10*).

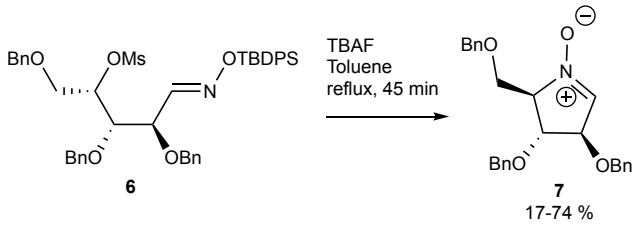

Scheme 10. Cyclisation of 6 to form zwitterion 7.

To produce the cyclic structure **7** the silyl protecting group in the acyclic compound **6** was removed by TBAF in refluxing toluene (*Scheme 10*). Presumably, this led to the formation of a reactive intermediate **6a** (*Scheme 11*), in which the nucleophilicity of the nitrogen atom is sufficient to facilitate the intramolecular stereospecific S_N2 substitution in the 4-position to form compound **7**. An S_N2 reaction is characterized by the synchronous formation of a new bond and the cleavage of an old one to give a 5-coordinate carbon transition state which rapidly falls apart to give the reaction product. In chiral molecules, an inversion of stereochemistry is further observed.

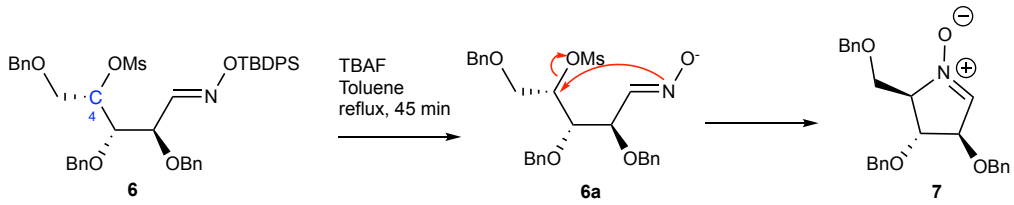

Scheme 11. Mechanism of the deprotection to form zwitterion 7.

This reaction was performed two times due to the poor results of 17% yield the first time. The reason being for the poor results the first time was proposed to be due to the usage of wet toluene. The water in toluene affects TBAFs ability to desilyate, possibly by creating a cage around the fluoride ion and disabling its effect. It has been shown from literature, that the desilylation efficiency of TBAF is greatly dependent by the water content of the TBAF reagent, and it should be 5% or less.[33] The second time this reaction was performed, anhydrous toluene was employed resulting in compound **7** being obtained in a yield of 74%.

2.1.5 Reduction and deoxygenation reaction

The main goal behind of this reaction sequence was to reduce the imine oxide moiety of compound **7** in two consecutive steps to afford amine **9** (*Scheme 12*).

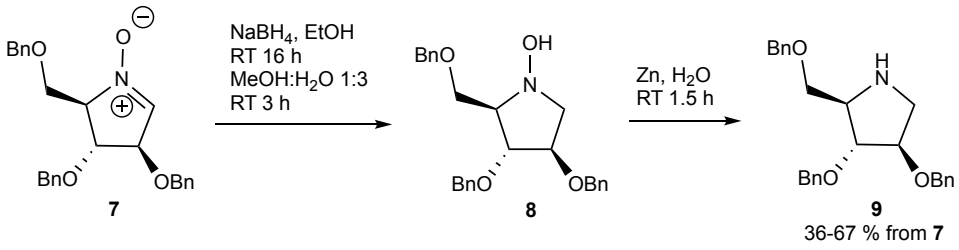

*Scheme 12. Reduction and deoxygenation reaction to furnish compound **9**.*

Imine oxide **7** underwent a $NaBH_4$/Zn reduction sequence via hydroxylamine **8** to provide pyrrolidine **9** in 67% yield (*Scheme 13*). The mechanism for the reduction with Zn is currently not fully understood.

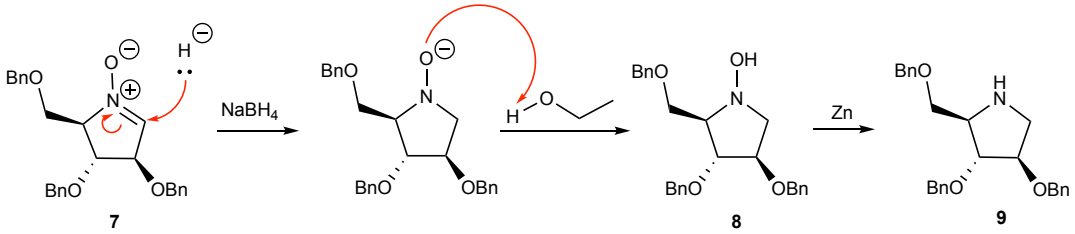

Scheme 13. Mechanism of the reduction of compound 7.

2.1.6 Formation of the target *N*-spiro fused compound 10 *via* double substitution reaction

This reaction was performed with the motivation to create the target *N*-spiro fused compound **10** via a double substitution reaction with 1,4-dibromobutane under basic conditions (*Scheme 14*). This reaction was performed two times with two different kinds of bases. The first time this reaction was performed Et_3N was chosen as the base for the deprotonation of the amine. The target molecule was synthesized, but the NMR-spectra showed impurity of the Et_3N salt (*Figure 8*) that could not be separated from **10** by silica column chromatography, which resulted in an incorrect mass balance and a yield exceeding 100%. The second time this reaction was performed NaOAc was used as a base for the deprotonation of the amine, which yielded the compound **10** in 77% with few impurities.

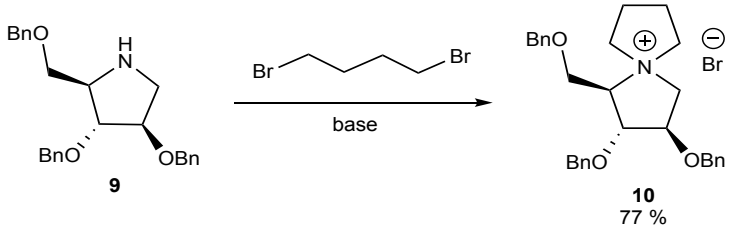

*Scheme 14. N-Spiro cyclization of pyrrolidine **9** with 1,4-dibromobutane to yield **10**.*

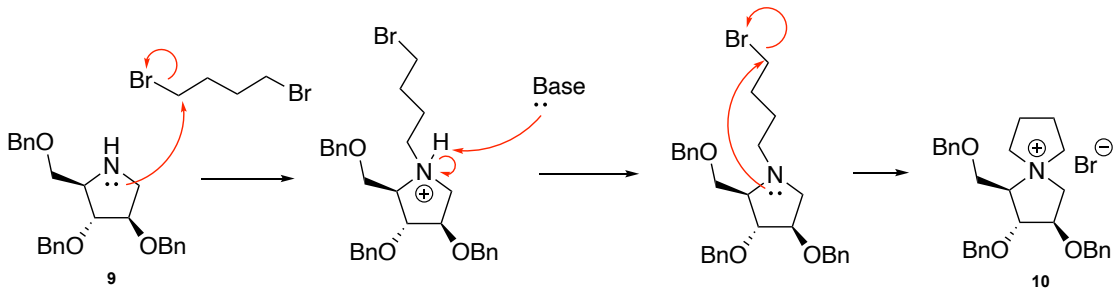

*Scheme 15. Proposed mechanism for the formation of compound **10**.*

The formation of *N*-spiro fused compound **10** occurs via a double substitution reaction (*Scheme 15*). The first step in the reaction is a nucleophilic attack by the lone pair electrons on the amine to the most electrophilic carbon on the alkyl halide. Then a base deprotonates the amine making the lone pair electrons on the amine available to initiate a second nucleophilic attack onto the alkyl chain, yielding compound **10** (*Scheme 15*).

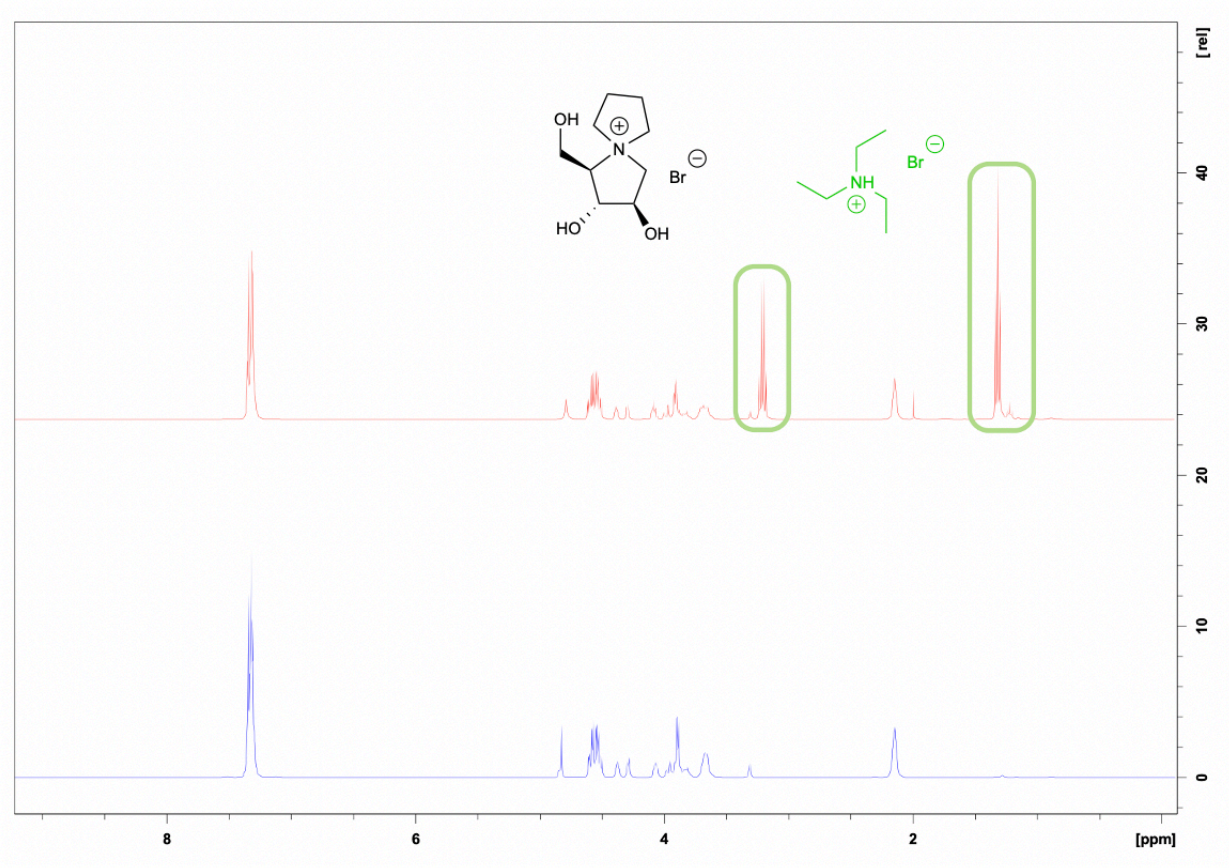

*Figure 8. [1]H-NMR-spectra of compound **10** showing both the pure compound and the compound with impurities. The red spectrum on the top shows compound **10** with the impurities highlighted by the green columns and the blue spectrum on the bottom shows the pure compound **10**.*

2.1.7 Benzyl deprotection to furnish target molecule 11

The sole purpose of this reaction was to remove the benzyl protecting groups and to furnish the target molecule **11** (*Scheme 16*)**.** The target molecule was obtained in quantitative yield**.** The Pd/C-catalyzed hydrogenation is often used for the removal of *O*-benzyl protective groups as a green sustainable method due to the easy removal and reuse of the catalyst. However, due to the strong coordination ability of amines to Pd, the catalytic activity gradually decreases depending on the extended contact time of the amines and Pd. Therefore, the usage of high pressure, high temperatures or acid catalysts can enhance the reaction rate and complete the deprotection. Addition of acetic acid and hydrochloric acid is believed to delay the poisoning rate of Pd/C.[34]

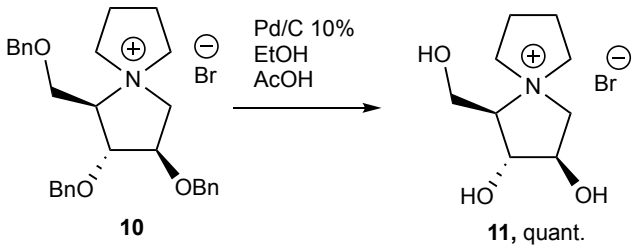

*Scheme 16. Benzyl deprotection to furnish target molecule **11**.*

The palladium-on-carbon (Pd/C)-catalyzed hydrogenative deprotection of the *O*-benzyl groups was facilitated using a EtOH-AcOH solvent system (*Scheme 16*). This reaction was done both with and without acetic acid. The results showed that the presence of acetic acid was instrumental in the conversion of the starting material into the target molecule.

2.2 Concluding remarks

The *N*-spiro fused quaternary ammonium salt **11** was successfully synthesized in 7 steps with L-xylose as the starting material. Thus, the synthesis was commenced from L-xylose, which underwent a Fischer glycosylation benzylation-hydrolysis sequence to provide tri-*O*-benzylated furanose **3** in 46% yield over three steps. With furanose **3** in hand, a nitrogen nucleus in the form of an oxime group was incorporated in the anomeric position of **3** to provide an aldoxime **4**, which underwent regioselevtive *O*-silylation to afford the silylether **5** in 48% yield. In order to facilitate a good leaving group for the ring closure of compound **5**, the hydroxyl group in the 4-position underwent *O*-mesylation to afford mesylate **6** in 86% yield, which in turn underwent cyclization into zwitterion **7** when the silyl protecting group was removed in refluxing toluene in the presence of TBAF. The usage of anhydrous toluene yielded good results (74%) in comparison to wet toluene (17%) which yielded poor results due to the presence of water in contact with the TBAF reagent. Reduction and deoxygenation were performed on the zwitterion **7** to furnish pyrrolidine **9** (67%). The *N*-spiro fused compound **10** was obtained by using 1,4 – dibromobutane and Et_3N (104%). The ^{1}H- NMR-spectra of **10** showed the impurities of the salt of Et_3N which further led to the usage of a non-organic base NaOAc instead of Et_3N yielding the compound **10** with no impurities (77%). In the final step, the benzyl groups were removed by employing palladium-catalyzed hydrogenation to afford the target compound **11** in quantitative yield.

2.3 Future work

We believe that our developed strategy to obtain compound **11** is applicable to synthesize an expanded library of spirocyclic ammonium compounds, which are also of pharmaceutical interest as potential acetylcholinesterase inhibitors. Compound **11** will undergo biological testing as a potential acetylcholinesterase inhibitor by Associate Professor Óscar Lopéz at the University of Seville.

3 Experimental

3.1 General

3.1.1 Solvents and reagents

All chemicals that were used for the procedures were obtained from Merck, VWR or Sigma Aldrich and used as supplied unless otherwise stated in the experimental procedures.

3.1.2 Spectroscopic and spectrometric analysis

Nuclear magnetic resonance (NMR) spectra were recorded on the Bruker Ascend ^{TM} 400 series, operating at 400 MHz for ^{1}H and MHz for ^{13}C, respectively. The chemical shifts (δ) are expressed in ppm relative to residual chloroform-d (^{1}H, 7.26 ppm; ^{13}C, 77.16 ppm), D_2O (^{1}H, 4.79 ppm) and CD_3OD (^{1}H, 3.31 ppm; ^{13}C, 49.00 ppm). Coupling constants (*J*) are given in Hertz (Hz) and the multiplicity is reported as: singlet (s), doublet (d), triplet (t), doublet of doublets (dd), multiplet (m) and broad singlet (brs). The assignments of signals in various NMR spectra were often assisted by conducting heteronuclear single-quantum correlation spectroscopy (HSQC) and/or heteronuclear multiple bond correlation spectroscopy (HMBC). Infrared (IR) spectra were recorded on the Agilent Cary 630 FTIR spectrometer. The samples were analyzed by direct placement onto the crystals of an attenuated total reflectance (ATR) module.[35]

3.1.3 Chromatography

Thin-layer chromatography (TLC) was carried out using aluminum backed 0.2 mm silica gel plates. The spots of the product were detected using ultraviolet (UV) extinction at λ=254 nm or λ=366 nm. Flash column chromatography (FCC) was also carried out with silica gel, with solvent gradients that are indicated in the procedure. Flash chromatography (FC) was carried out with silica gel (particle size 40-63 μm), with solvent gradients as indicated in the experimental procedures.

3.2 Methods

3.2.1 2,3,5-Tri-*O*-benzyl-L-xylofuranose (3)

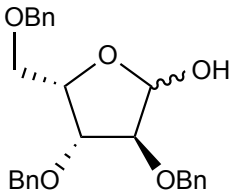

AcCl (0.47 mL, 6.66 mmol, 0.2 equiv) was added dropwise to MeOH (70mL) before addition of L-xylose (5.0 g, 33.3 mmol, 1.0 equiv). The obtained mixture was kept stirring at RT for 5.5 h. The temperature was then adjusted to 0°C before dropwise addition of aq NaOH (1M) until basic pH (8-9) was reached. The solvent was removed under reduced pressure and the resulting concentrate was co-evaporated three times from toluene. The residue was dissolved in anhyd DMF (106 mL) and NaH (60% dispersion in mineral oil, 7.3g, 176 mmol, 5.3 equiv) was added portionwise. The resulting suspension was kept stirring at RT under an argon atmosphere for 10 min. The temperature was then decreased to 0°C and BnBr (20 mL, 167 mmol, 5.0 equiv) was added dropwise. The mixture was then kept stirring overnight at RT. The temperature was adjusted to 0°C before dropwise addition of H_2O (167 ml). The aqueous mixture was extracted with EtOAc (2 x 167 mL) and the combined organic layers were dried ($MgSO_4$), filtered, and concentrated under reduced pressure. The residue was dissolved in 1,4-dioxane (100 mL) and aq HCl (100 mL 4 M) and the mixture was kept stirring at 60-65°C for 2 days. The aqueous mixture was extracted with EtOAc (2 x 125 mL) and the combined organic layers were concentrated under reduced pressure. The residue was purified by silica gel flash column chromatography (PE-EtOAc, 4:1 → 7:3, v/v) to provide 6.41 g (46%) of a colorless syrup.[29]

$\boldsymbol{R_f}$ = 0.35 (PE-EtOAc, 4:1, v/v)

IR (ATR): ν_{max} 3447, 3063, 3029, 2921, 2865, 1734, 1453, 1053, 733 cm^{-1}.

^{1}H-NMR ($CDCl_3$, 400 MHz) δ: 3.60-3.71 (m, 2.4H) 3.83-3.88 (m, 1.2H), 3.93-3.97 (m, 1.2H), 4.02-4.04 (m, 0.8H), 3.31-4.33 (m, 1,2H), 4.41-5.57 (m, 5.6H), 5.16-5.19 (m, 0.8H), 5.40 (dd, 0.4H, *J* = 4.0 Hz, *J* = 9.2 Hz), 7.17-7.31 (m, 15H).

^{13}C-NMR ($CDCl_3$, 100 MHz) δ: 68.4, 68.8, 72.0, 72.2, 72.4, 72.8, 73,2, 73.6, 73.8, 77.5, 80.0, 81.1, 81.4, 86.7, 96.3, 101.8, 127.7-128.8 (aromatic carbons), 137.5, 137.6, 137.7, 137.8, 138.3, 138.4.

3.2.2 (2*R*,3*R*,4*S*,*E*)-2,3,5-Tris(benzyloxy)-4-hydroxypentanal *O*-(*tert*-butyldiphenylsilyl) oxime (5)

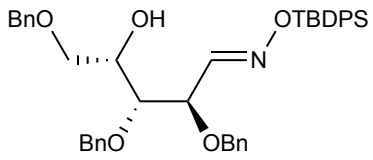

A solution of sodium methoxide methanol *in situ* (9 mL, 44.4 mmol, 4 equiv) was added to a solution of **3** (4.68 g, 11.1 mmol, 1.0 equiv) and hydroxylamine hydrochloride (6.19 g, 88.8 mmol, 8.0 equiv) in MeOH (70 mL). The obtained mixture was kept stirring at RT for 2 h before the solvent was removed under reduced pressure. The residue was dissolved in 100 mL of water and 100 mL of EtOAc, then the phases were separated, and the organic extract was dried, filtered and concentrated. The crude product was further dissolved in toluene and concentrated under reduced pressure two times, before DCM (24 mL) and imidazole (0.98 g, 14.5 mmol, 1.3 equiv) were added to the solution. After this, TBDPS-Cl (3.60 mL, 13.9 mmol, 1.25 equiv) was added portionwise and the resulting mixture was kept stirring at RT for 30 min. The mixture was then diluted by addition of water/DCM (50 mL, 1:1 v/v) and extracted with DCM (3 x 50 mL). The combined organic phases were dried ($MgSO_4$), filtered and concentrated under reduced pressure. Purification by flash column chromatography (PE-EtOAc, 9:1 → 17:3, v/v) yielded 4.06 g (54%) of a yellow oil.[36]

R_f = 0.11 (PE-EtOAc, 9:1, v/v)

IR (ATR): ν_{max} 3500, 3030, 2930, 2857, 1736, 1453, 1239, 912, 694 cm^{-1}.

The ^{13}C NMR and ^{1}H NMR for compound **5** was never properly assigned as it decomposed in the NMR solvent ($CDCl_3$), presumable due to the presence HCl residues. In addition, compound **5** exists as a mixture of two isomers, which further complicates the assignment of the NMR spectra.

3.2.3 (2*R*,3*R*,4*S*,*E*)-2,3,5-Tris(benzyloxy)-4-metylsulfonyloxypentanal *O*-(*tert*-butyldiphenylsilyl) oxime (6)

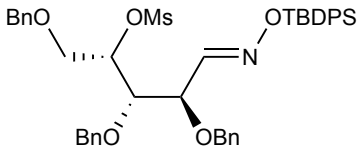

MsCl (0.3 mL, 3.84 mmol, 1.17 equiv) and NEt_3 (0.7 mL, 5.08 mmol, 1.5 equiv) were slowly added to a solution of **5** (2.21g, 3.28 mmol, 1.0 equiv) in DCM (10 mL) under an argon atmosphere at 0°C. The mixture was kept stirring for 30 minutes, before water (2.7 mL) was added. Then the mixture was diluted by addition of water/DCM (20 mL, 1:1 v/v) and extracted with DCM (3 x 20 mL). The organic layers were then dried ($MgSO_4$) and concentrated under reduced pressure. Purification by flash column chromatography (PE-EtOAc, 7:1 → 33:7, v/v) yielded 2.13 g (86%) of a yellow oil.[37]

$\boldsymbol{R_f}$ = 0.42 (PE-EtOAc, 7:1, v/v)

IR (ATR): ν_{max} 3030, 2931, 2858, 1735, 1357, 1175, 910, 695 cm^{-1}.

The ^{13}C NMR and ^{1}H NMR for compound **6** was never properly assigned as it decomposed in the NMR solvent ($CDCl_3$), presumable due to the presence HCl residues. In addition, compound **6** exists as a mixture of two isomers, which further complicates the assignment of the NMR spectra.

3.2.4 (2*R*,3*R*,4*R*)-3,4-Bis(benzyloxy)-2-((benzyloxy)methyl)-3,4-dihydro-2*H*-pyrrole 1-oxide (7)

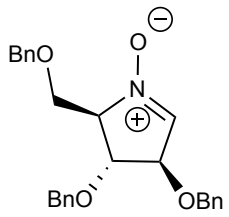

TBAF (7,07 mL, 1M in THF, 7.068 mmol, 1.55 equiv) was slowly added to a solution of **6** (3.43 g 4.56 mmol, 1.0 equiv) in toluene (56 mL). The reaction was then heated to reflux for 45 minutes before being allowed to cool to RT. The residues were taken up in DCM (30 mL), water (60 mL) was added to the aqueous phase and extracted with DCM (3 x 30 mL), before the combined organic layers were concentrated under reduced pressure. Purification by flash column chromatography (PE-EtOAc-MeOH, 1:1:0 → 0:1:0 → 0:39:1, v/v) yielded 1.41 g (74 %) of a white powder.[36]

R_f = 0.59 (PE-EtOAc, 1:1, v/v)

IR (ATR): ν_{max} 3166, 3049, 2922, 2883, 1591, 1275, 1086, 696 cm^{-1}.

^{1}H-NMR ($CDCl_3$, 400 MHz) δ_H: 3.70 (dd, 1H, *J* = 2.3 Hz, *J* = 10.0 Hz), 3.93-3.99 (m, 2H), 4.30 (dd, 1H, *J* = 2.2 Hz, *J* = 3.5 Hz), 4.23-4.50 (m, 5H), 4.54 (d, 1H, *J* = 12.0 Hz), 4.59-4.60 (m, 1H), 6.82 (brs, 1H), 7.19-7.29 (m, 15H)

^{13}C-NMR ($CDCl_3$, 100 MHz) δ_C: 66.3, 71.8, 72.1, 73.6, 77.6, 80.5, 83.0, 127.8, 127.9, 128.0, 128.1, 128.3 (2xC), 128.5, 128.7 (2xC), 132.9, 137.3, 137.4, 137.8

3.2.5 (2*R*,3*R*,4*R*)-3,4-Bis(benzyloxy)-2-((benzyloxy)methyl)pyrrolidine (9)

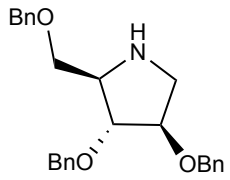

$NaBH_4$ (0.26 g, 6.76 mmol) was added to a solution of **7** (1.41 g, 3.38 mmol, 1.0 equiv) in 68 ml of EtOH. The mixture was stirred at RT for 16 h, until a TLC analysis (PE-EtOAc, 1:1, v/v) showed the disappearance of the starting material (R_f = 0.50) and the formation of a new product (R_f = 0.80). MeOH (5.6 mL) and water (16.9 mL) water were then added. The mixture was allowed to warm to RT and stirred for another 3 h, before it was evaporated under reduced pressure and the crude obtained was filtered through Celite by the aid of diethyl ether. The collected filtrate was evaporated under reduced pressure. The residue was dissolved in 45 mL of acetic acid, before Zn powder (3.57 g, 54.6 mmol, 20.0 equiv) and water (45 mL) were added. The reaction mixture was stirred at RT for 1.5 h until a TLC analysis (DCM-MeOH, 39:1, v/v) showed the disappearance of the starting material (R_f = 0.43) and the formation of a new product (R_f = 0.34). The mixture was filtrated through cotton, concentrated under reduced pressure and then saturated aqueous solution of Na_2CO_3 was added at 0°C until basic pH was realized. After extraction with EtOAc (3 x 30 mL), the organic layers were concentrated under reduced pressure and the crude was purified by flash column chromatography (DCM-EtOAc, 1:1 → 13:7, v/v) to yield 910 mg (67 %) of colorless oil.[38]

***R*$_f$** = 0.082 (DCM-EtOAc, 1:1, v/v)

IR (ATR): ν_{max} 3062, 2857, 1453, 1363, 1071, 907, 731, 694 cm^{-1}.

^{1}**H-NMR** ($CDCl_3$, 400 MHz) δ_H: 2.15 (brs, 1H), 3.01 (d, 2H, J = 3.1 Hz), 3.15-3.17 (m, 1H), 3.46-3.55 (m, 2H), 3.79-3.80 (m, 1H), 3.93 (brs, 1H), 4.36-4.49 (m, 6H), 7.16-7.27 (m, 15H)

^{13}C-NMR ($CDCl_3$, 100 MHz) δ_C: 51.2, 64.3, 70.5, 71.2, 72.0, 73.3, 84.7, 85.9, 127.7-128.5 (aromatic carbons), 138.3 (2xC), 138.4

3.2.6 (1*R*,2*R*,3*R*)-2,3-Bis(benzyloxy)-1-((benzyloxy)methyl)-5-azaspiro[4.4]nonan-5-ium-bromide (10)

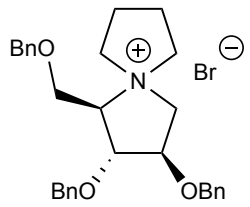

Method 1. To a solution of **9** (69.5 mg, 0.17 mmol, 1.0 equiv) in THF (2.5 mL), NEt_3 (118 µL, 0.85 mmol, 5 equiv) and 1,4 – dibromobutane (124 µL, 1.037 mmol, 6.1 equiv) were added. The reaction mixture was stirred at RT for 6 days until a TLC analysis (DCM-MeOH, 4:1, v/v) showed the disappearance of the starting material (R_f = 0.89) and the formation of a new product (R_f = 0.80). MeOH was then added, and the solution was evaporated under reduced pressure. The crude was purified by flash column chromatography (DCM-MeOH, 19:1 → 9:1, v/v) to provide 145 mg (104 %) of a mixture containing 54% of **10** and 46% of the salt of triethylamine which was verified from ^{1}H NMR spectroscopy.

Method 2. To a solution of **9** (104 mg, 0.26 mmol, 1.0 equiv) in THF (5 mL), NaOAc (107 mg, 1.3 mmol, 5 equiv) and 1,4 – dibromobutane (200 µL, 1.6 mmol, 6.1 equiv) were added. The reaction mixture was stirred at RT for 6 days until a TLC analysis (DCM-MeOH, 4:1, v/v) showed the disappearance of the starting material (R_f = 0.82) and the formation of a new product (R_f = 0.71). MeOH was then added, and the solution was evaporated under reduced pressure. The crude was purified by flash column chromatography (DCM-MeOH, 19:1 → 187:13, v/v) to yield 108 mg (77 %) of a white crystal.

***R*$_f$** = 0.23 (DCM-MeOH, 19:1, v/v)

IR (ATR): ν_{max} 3030, 2939, 2869, 1454, 1096, 1023, 729 cm^{-1}.

^{1}**H-NMR** (CD_3OD, 400 MHz) δ_H: 2.15 (s, 4H), 3.65-3.70 (m, 3H), 3.79-3.99 (m, 5H), 4.05-4.09 (m, 1H), 4.29 (dd, 1H, J=1.7, J=5.8), 4.37 (brs, 1H), 4.50-4.61 (m, 6H), 7.31-7.34 (m, 15H)

^{13}**C-NMR** (CD_3OD, 100 MHz) δ_C: 22.1, 22.9, 60.3, 66.0, 66.9, 67.5, 73.1, 73.3, 74.4, 76.7, 81.2, 84.2, 129.1-129.6 (aromatic carbons), 138.3 (2xC), 138.5

3.2.7 (1*R*,2*R*,3*R*)-2,3-Dihydroxy-1-(hydroxymethyl)-5-azaspiro[4.4]nonan-5-ium-bromide (11)

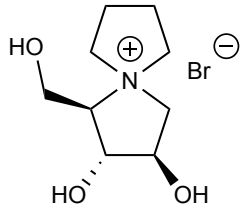

Compound **10** (16.4 mg, 0.0300 mmol, equiv 1) dissolved in EtOH (2 mL) was added 10 wt% of Pd/C (35 mg). The obtained mixture was kept stirring under a hydrogen atmosphere at 30 °C for 2 days. After this time acetic acid (2 mL) was added, and the reaction mixture was then stirred under a hydrogen atmosphere at 30 °C for another 4 days. The reaction mixture was then filtered through Celite and EtOH was evaporated. The total yield of this reaction was 14.7 mg in quantitative yield.

IR (ATR): ν_{max} 3276, 2924, 2853, 1570, 1412, 1082, 925, 731 cm^{-1}.

^{1}H-NMR (D_2O, 400 MHz) δ_H: 2.14-2.27 (m, 4H), 3.60-3.90 (m, 7H), 4.13 (d, 2H, J=4.7 Hz), 4.31 (dd, 1H, J=3.7 Hz, J=6.9 Hz), 4.48-4.49 (m, 1H)

^{13}C-NMR (D_2O, 100 MHz) δ_C: 20.4, 20.9, 57.1, 59.2, 66.6, 67.3, 73.6, 76.8, 77.1

References

1. Breijyeh, Z. and R. Karaman, Comprehensive Review on Alzheimer's Disease: Causes and Treatment. *Molecules*, 2020. **25(24)**, 5789.
2. National Institute on Aging, *What Is Dementia? Symptoms, Types, and Diagnosis,* 2017, Available from Https://Www.Nia.Nih.Gov/Health/What-Dementia-Symptoms-Types-and-Diagnosis, Accessed 21 April 2021.
3. Sharma, K., Cholinesterase Inhibitors as Alzheimer´S Therapeutics (Review). *Mol. Med. Rep.*, 2019. **20**, 1479-1487.
4. Querfurth, H.W. and F.M. LaFerla, Alzheimer´S Disease. *N. Engl. J. Med.*, 2010. **362**, 329-344.
5. Alzheimer's Disease International, *Dementia Statistics*, 2017, Available from Https://Www.Alzint.Org/About/Dementia-Facts-Figures/Dementia-Statistics/, Accessed 21 April 2021.
6. Alzheimer's News Today, *Alzheimer's Disease Statistics*, Available from Https://Alzheimersnewstoday.Com/Alzheimers-Disease-Statistics/, Accessed 21 April 2021.
7. Norwegian Institute of Public Health, *Dementia in Norway*, 2015, Available from Https://Www.Fhi.No/En/Op/Hin/Health-Disease/Dementia-in-Norway/, Accessed 21 April 2021.
8. Menon Economics, *Alzheimers Og Annen Demens Koster Samfunnet 100 Milliarder Kroner, Dobles De Neste 20 Årene*, 2020, Available from Https://Www.Menon.No/Alzheimers-Annen-Demens-Koster-Samfunnet-100-Milliarder-Kroner-Dobles-Neste-20-Arene/, Accessed 21 April 2021.
9. Cimler, R., P. Maresova, J. Kuhnova, and K. Kuca, Predictions of Alzheimer's Disease Treatment and Care Costs in European Countries. *PLoS ONE*, 2019. **14**, e0210958.
10. Goedert, M., Oskar Fischer and the Study of Dementia. *Brain*, 2009. **132**, 1102-1111.
11. Savelieff, M.G., G. Nam, J. Kang, H.J. Lee, M. Lee, and M.H. Lim, Development of Multifunctional Molecules as Potential Therapeutic Candidates for Alzheimer's Disease, Parkinson's Disease, and Amyotrophic Lateral Sclerosis in the Last Decade. *Chem. Rev.*, 2019. **119**, 1221-1322.
12. Rajmohan, R. and P. Hemachandra Reddy, Amyloid Beta and Phasphorylated Tau Accumulations Cause Abnormalities at Synapses of Alzheimer's Disease Neurons. *J. Alzheimers Dis.* , 2017. **57**, 975-999.
13. Hroudová, J., N. Singh, Z. Fišar, and K.K. Ghosh, Progress in Drug Development for Alzheimer's Disease: An Overview in Relation to Mitochondrial Energy Metabolism. *Eur. J. Med. Chem.*, 2016. **121**, 774-784.
14. Alzheimer's Association, *2016 Alzheimer's Disease Facts and Figures*, 2016, Available from Https://Alz-Journals.Onlinelibrary.Wiley.Com/Doi/Full/10.1016/J.Jalz.2016.03.001, Accessed 21 April 2021.

15. Alzheimer's Association, *Can Alzheimer's Disease Be Prevented?*, Available from Https://Www.Alz.Org/Alzheimers-Dementia/Research_Progress/Prevention, Accessed 21 April 2021.

16. Alzheimer's Association, *Causes and Risk Factors for Alzheimer's Disease*, Available from Https://Www.Alz.Org/Alzheimers-Dementia/What-Is-Alzheimers/Causes-and-Risk-Factors, Accessed 21 April 2021.

17. Kozurkova, M., S. Hamulakova, Z. Gazova, H. Paulikova, and P. Kristian, Neuroactive Multifunctional Tacrine Congeners with Cholinesterase, Anti-Amyloid Aggregation and Neuroprotective Properties. *Pharmaceuticals*, 2011. **4(2)**, 382-418.

18. Bartus, R.T., R.L. Dean 3rd, B. Beer, and A.S. Lippa, The Cholinergic Hypothesis of Geriatric Memory Dysfunction. *Science*, 1982. **217**, 408-414.

19. Hampel, H., M.-M. Mesulam, A.C. Cuello, M.R. Farlow, E. Giacobini, G.T. Grossberg, A.S. Khachaturian, A. Vergallo, E. Cavedo, P.J. Snyder, and Z.S. Khachaturian, The Cholinergic System in the Pathophysiology and Treatment of Alzheimer's Disease *Brain*, 2018. **141**, 1917-1933.

20. Terry Jr, A.V. and J.J. Buccafusco, The Cholinergic Hypothesis of Age and Alzheimer's Disease - Related Cognitive Deficits: Recent Challenges and Their Implications for Novel Drug Development. *J. Pharmacol. Exp. Ther.*, 2003. **306**, 821-7.

21. Vijayan, D.K. and C. Remya, Amyloid Beta Hypothesis in Alzheimer's Disease: Major Culprits and Recent Therapeutic Strategies. *Curr. Drug Targets*, 2019. **20**, 000-000.

22. Xu, Y., J.-P. Colletier, M. Weik, H. Jiang, J. Moult, I. Silman, and J.L. Sussman, Flexibility of Aromatic Residues in the Active-Site Gorge of Acetylcholinesterase: X-Ray Versus Molecular Dynamics. *Biophys. J.*, 2008. **95(5)**, 2500-2511.

23. Sussman, J.L., M. Harel, O. Oefner, A. Goldman, L. Toker, and I. Silman, Atomic Structure of Actylcholinesterase from Torpedo Californica: A Prototypic Acetylcholine-Binding Protein. *Science*, 1991. **253**, 872-879.

24. De Santana, Q.L.O., T.C.S. Evangelista, P. Imhof, S.B. Ferreira, J.G. Fernández-Bolaños, M.O. Sydnes, Ó. Lopéz, and E. Lindbäck, Tacrine-Sugar Mimetic Conjugates as Enhanced Choliesterase Inhibitors. *Org. Biomol. Chem.*, 2021. **19**, 2322.

25. Tumiatti, V., A. Minarini, M.L. Bolognesi, A. Milelli, M. Rosini, and C. Melchiorre, Tacrine Derivates and Alzheimer's Disease. *Curr. Med. Chem.*, 2010. **17(17)**, 1825-1838.

26. Grider, M.H.J., R.; Glaubensklee, C. S. *Physiology, Action Potential;* (Updated 2020 Sep 10); In: StatPearls (Internet); Treasure Island (FL): StatPearls Publishing; 2021 Jan-; Available from : https://www.ncbi.nlm.nih.gov/books/NBK538143/

27. da Costa, J.S., D.S. Pisoni, C.B. da Silva, C.L. Petzhold, D. Russowsky, and M.A. Ceschi, Lewis Acid Promoted Friedländer Condensation Reactions between Anthranilonitrile and Ketones for the Synthesis of Tacrine and Its Analogues. *J. Braz. Chem. Soc.*, 2009. **20**, 1448-1454.

28. Tayeb, H.O., H.D. Yang, B.H. Price, and F.I. Tarazi, Pharmacotherapies for Alzheimer's Disease: Beyond Cholinesterase Inhibitors. *Pharmacology & Therapeutics*, 2012. **134**, 8-25.

29. Evangelista, T.C.S., Ó. Lopéz, M.O. Sydnes, J.G. Fernández-Bolaños, S.B. Ferreira, and E. Lindbäck, Bicyclic 1-Azafagomine Derivatives: Synthesis and Glycosidase Inhibitory Testing *Synthesis*, 2019. **51**, 4066-4077.

30. Aronow, J., C. Stanetty, I.R. Baxendale, and M.D. Mihovilovic, Methyl Glycosides Via Fisher Glycosylation: Translation from Batch Microwave to Continuous Flow Processing. *Monatsh. Chem.* , 2019. **150(1)**, 11-19.

31. Green, T.W. and P.G.M. Wuts, Protective Groups in Organic Synthesis, Third Edition. *John Wiley & Sons, Inc., Hoboken*, 1999, 17-245.

32. Master Organic Chemistry, *Tosylates and Mesylates*, Available from Https://Www.Masterorganicchemistry.Com/2015/03/10/Tosylates-and-Mesylates/, Accessed 2 May 2021.

33. Hogrefe R. I., M.A.P., Borozdina L. U., McCampbell E. S., Vaghefi M. M., Effect of Excess Water on the Desilylation of Oligoribonucleotides Using Tetrabutylammonium Fluoride. *Nucleic Acids Research* 1993. **21(20)**, 4739-4741.

34. Yamamoto, Y., E. Shimizu, K. Ban, Y. Wada, T. Mizusaki, M. Yoshimura, Y. Takagi, Y. Sawama, and H. Sajiki, Facile Hydrogentative Deprotection of *N*-Benzyl Groups Using a Mixed Catalyst of Palladium and Niobic Acid-on-Carbon *ACS Omega*, 2020. **5**, 2699-2709.

35. Fulmer, G.R., A.J.M. Miller, N.H. Sherden, H.E. Gottlieb, A. Nudelman, B.M. Stoltz, J.E. Bercaw, and K.I. Goldberg, Nmr Chemical Shifts to Trace Impurities: Common Laboratory Solvents, Organics, and Gases in Deuterated Solvents Relevant to the Organometallic Chemist. *Organometallics*, 2010. **29**, 2176-2179.

36. Rössler, S.L., B.S. Schreib, M. Ginterseder, J.Y. Hamilton, and E.M. Carreira, Total Synthesis and Stereochemical Assignment of (+)-Broussonetine H. *Org. Lett.*, 2017. **19**, 5533-5536.

37. Desvergnes, S., S. Py, and Y. Vallée, Total Synthesis of (+)-Hyacinthacine a_2 Based on Smi_2-Induced Nitrone Umpolung. *J. Org. Chem.*, 2005. **70**, 1459-1462.

38. D'Adamio, G., C. Matassini, C. Parmeggiani, S. Catarzi, A. Morrone, A. Goti, P. Paoli, and F. Cardona, Evidence for a Multivalent Effect in Inhibition of Sulfatases Involved in Lysosomal Storage Disorders (Lsds). *RSC ADV*, 201**6**. **6**.

4 Appendix

4.1 Spectra for compounds

4.1.1 2,3,5-Tri-*O*-benzyl-L-xylofuranose (3)

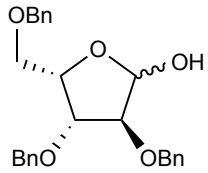

3

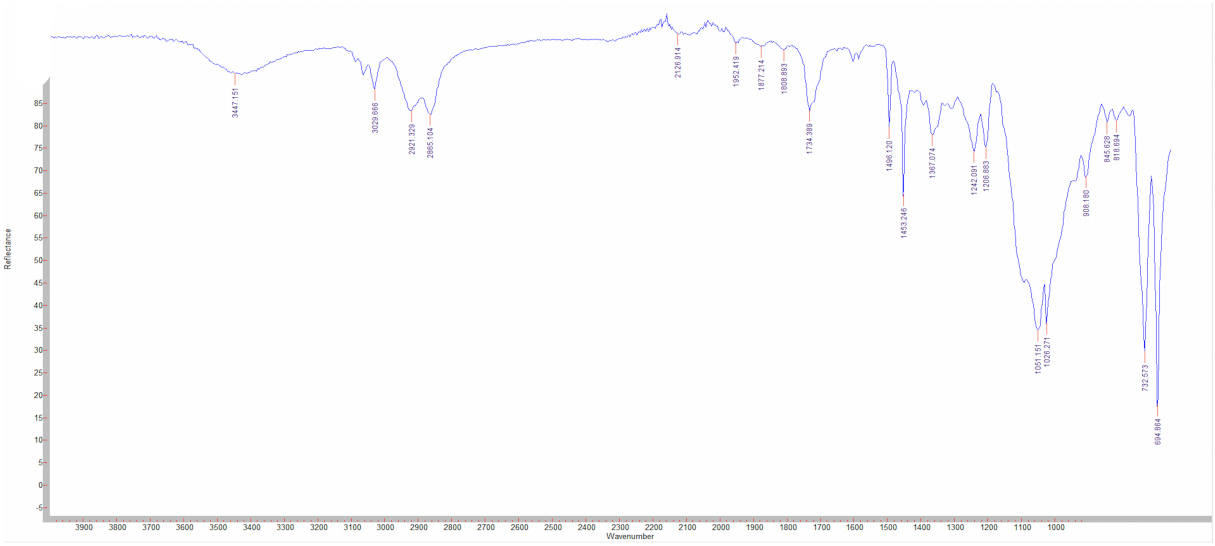

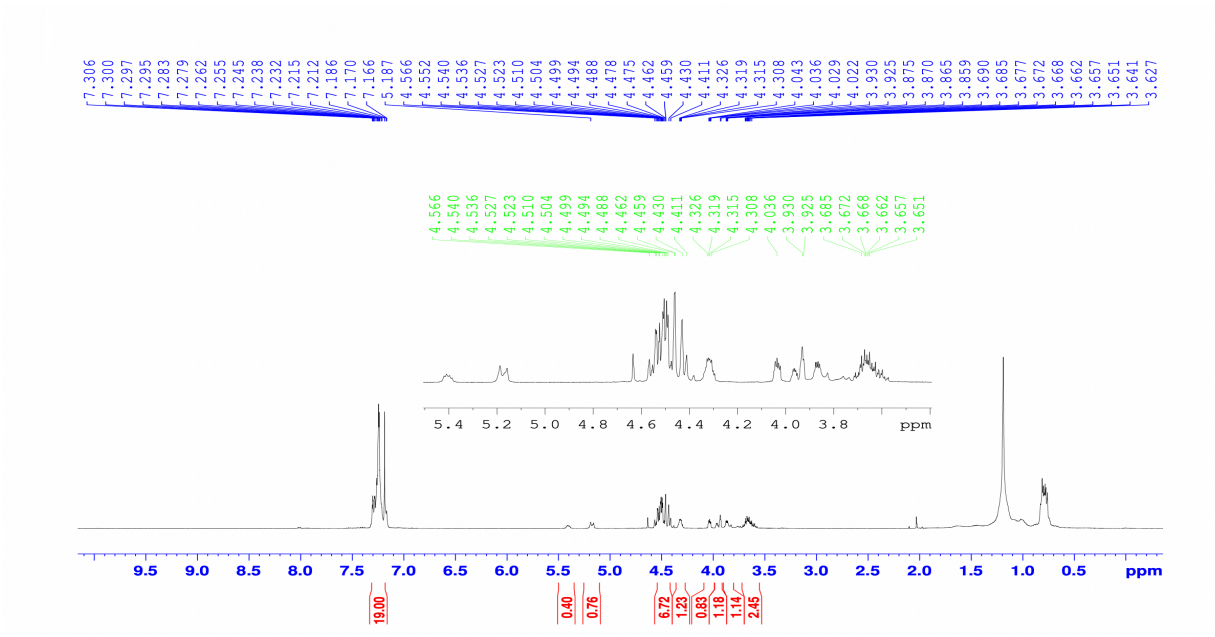

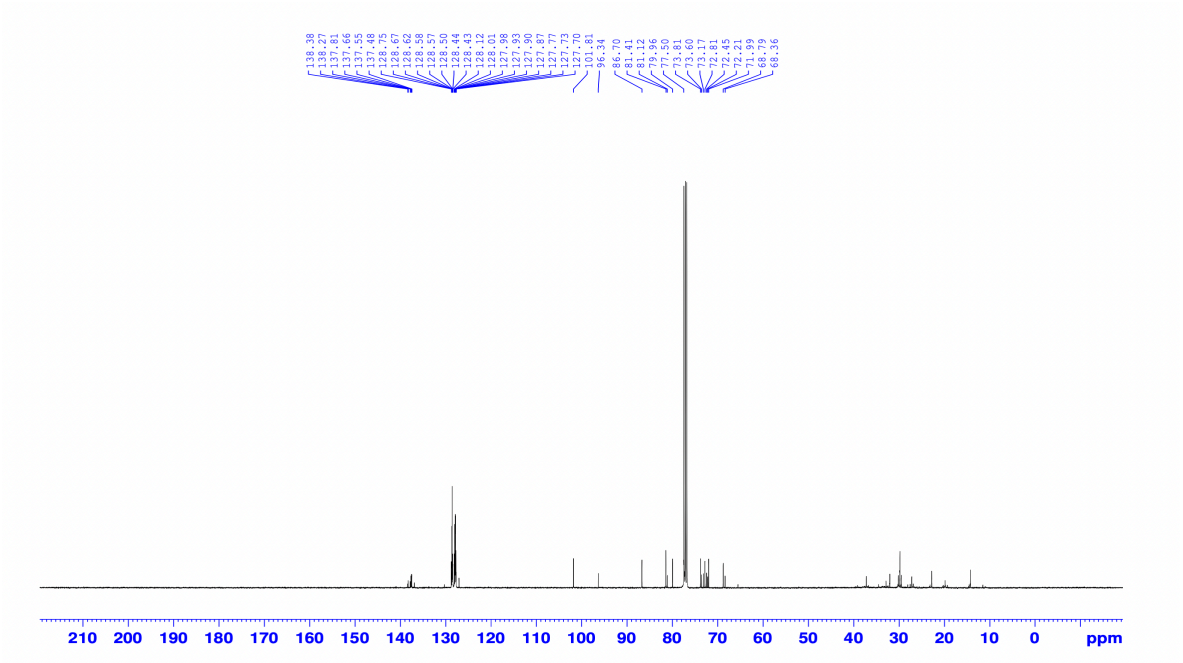
138.38
138.27
137.81
137.66
137.55
137.48
128.75
128.67
128.62
128.58
128.57
128.50
128.44
128.43
128.12
128.01
127.98
127.93
127.90
127.87
127.77
127.73
127.70
101.81
96.34
86.70
81.41
81.12
79.96
79.60
73.81
73.60
73.17
72.81
72.45
72.21
71.99
71.79
68.36
210 200 190 180 170 160 150 140 130 120 110 100 90 80 70 60 50 40 30 20 10 0 ppm

4.1.2 (2*R*,3*R*,4*S*, *E*) -2,3,5-Tris(benzyloxy)-4-hydroxypentanal *O*-(*tert*-butyldiphenylsilyl) oxime (5)

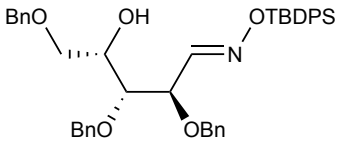

5

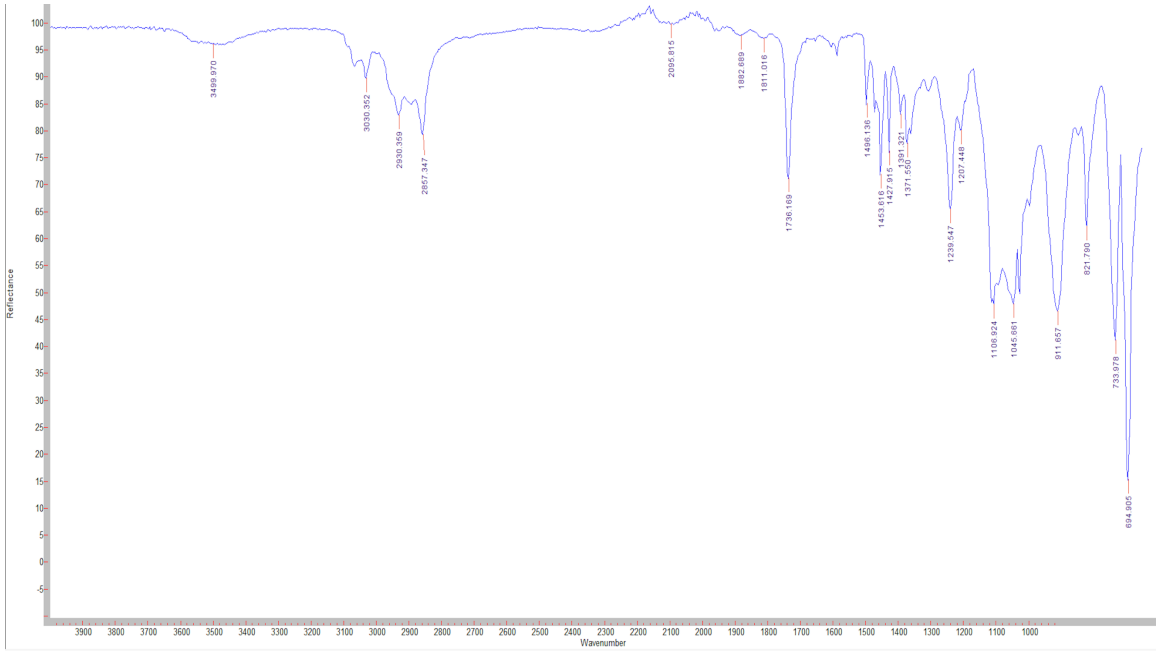

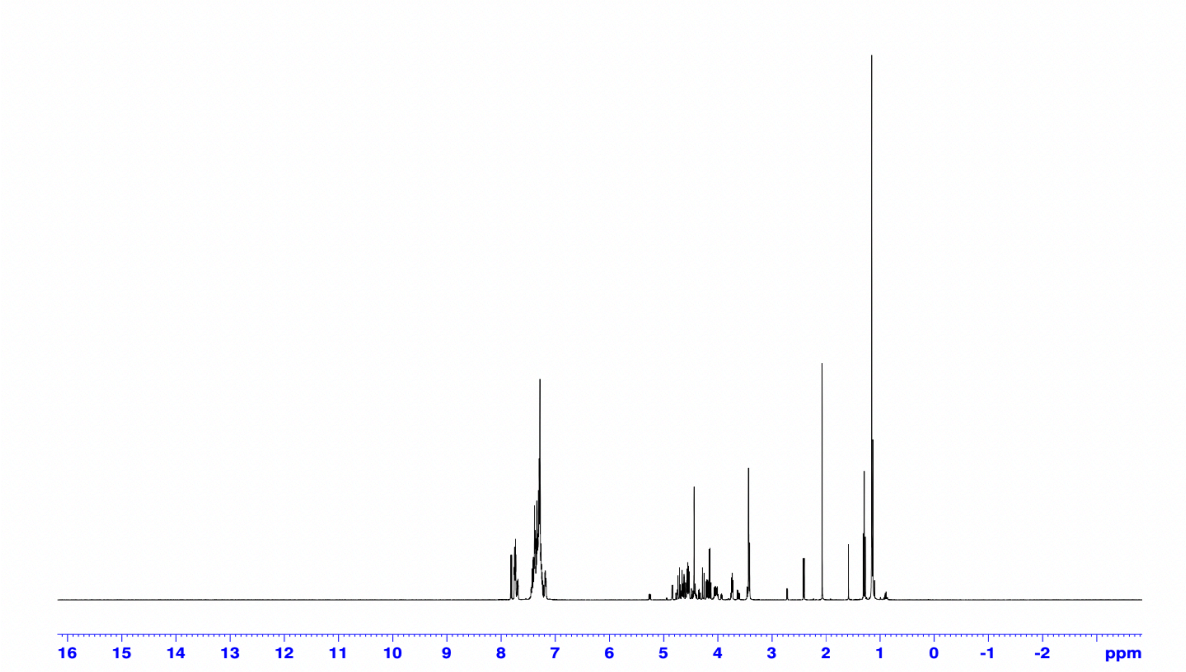

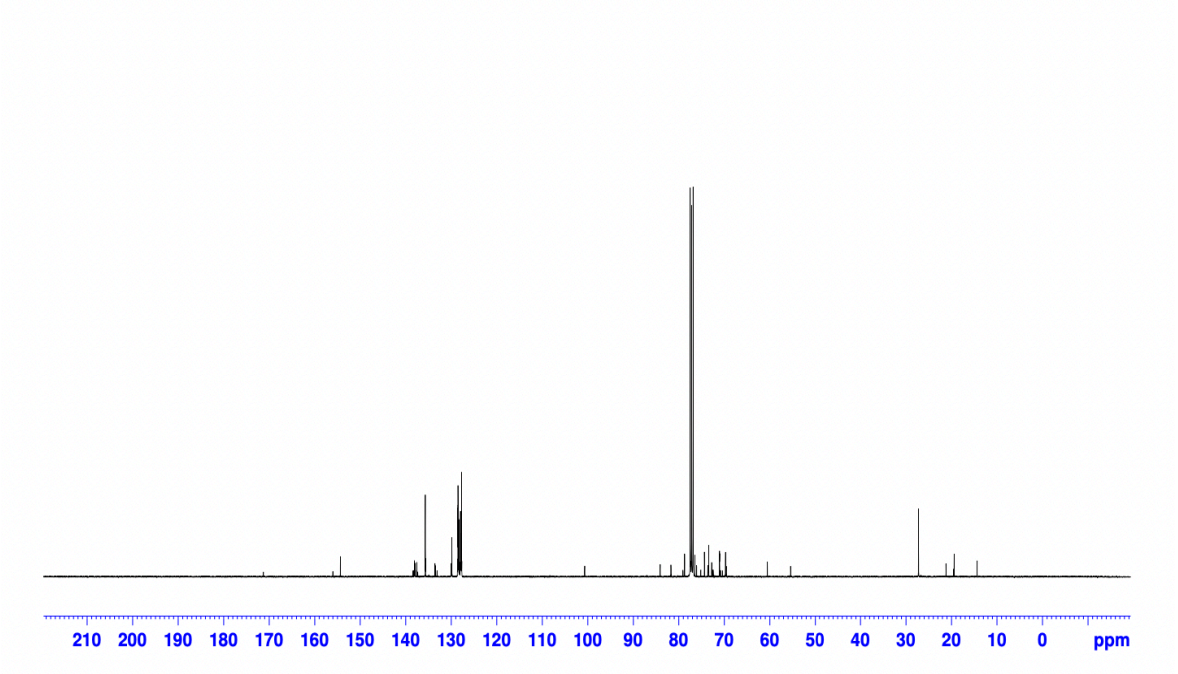
210 200 190 180 170 160 150 140 130 120 110 100 90 80 70 60 50 40 30 20 10 0 ppm

4.1.3 (2R,3R,4S, E)-2,3,5-Tris(benzyloxy)-4metylsulfonyloxypentanal O-(tert-butyldiphenylsilyl) oxime (6)

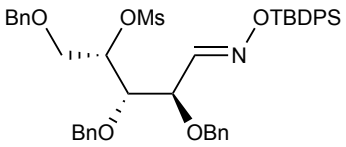

6

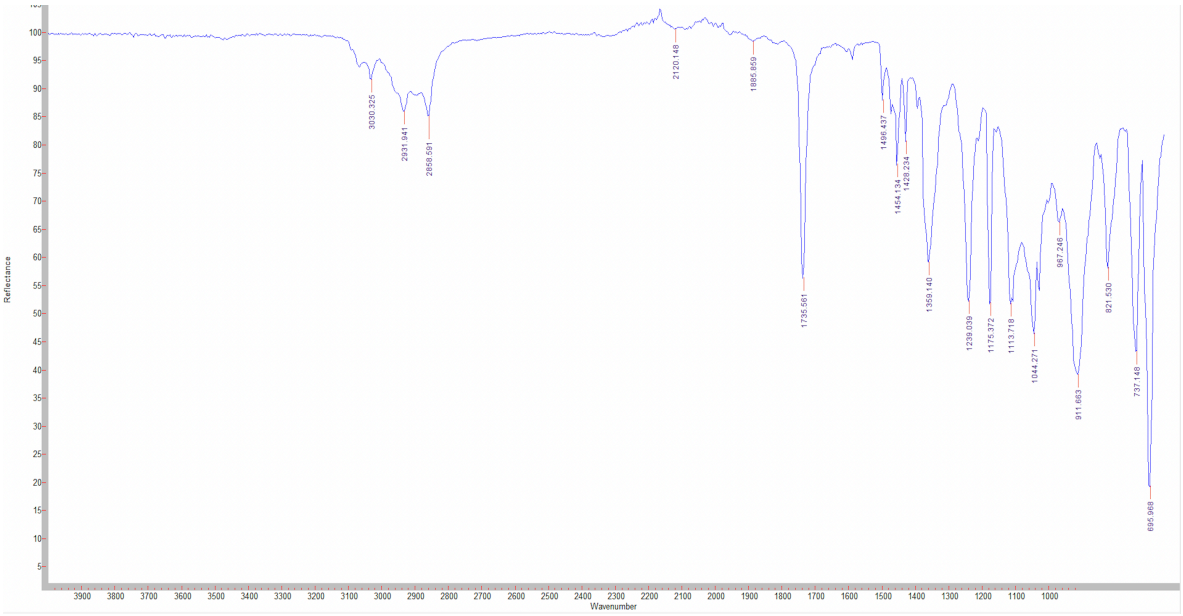

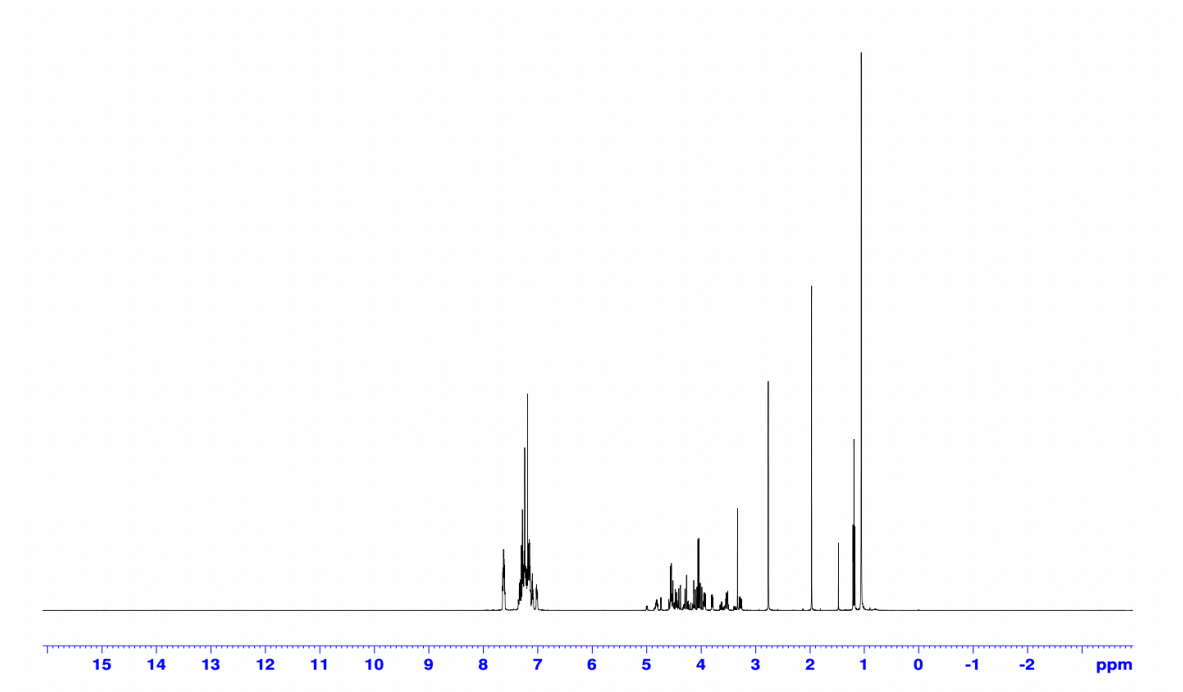

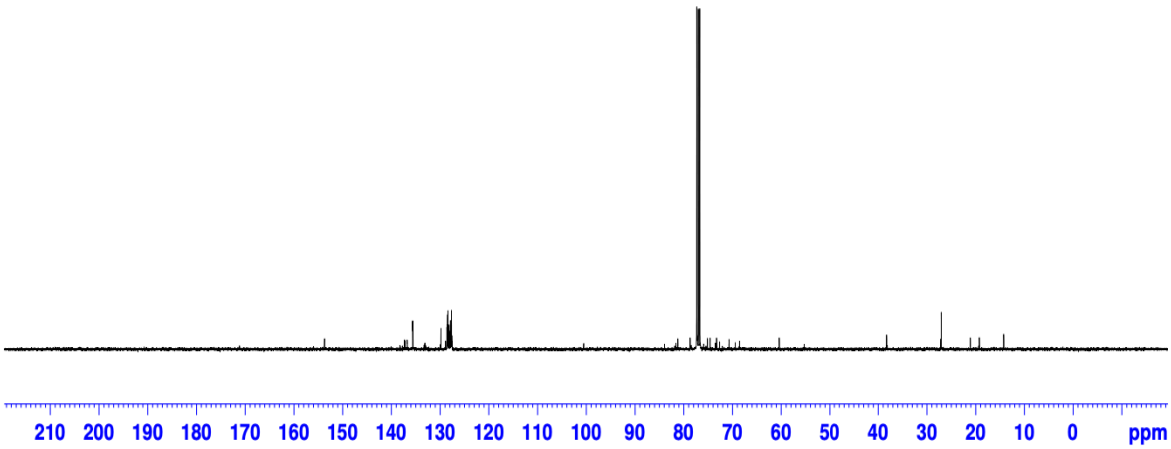
210 200 190 180 170 160 150 140 130 120 110 100 90 80 70 60 50 40 30 20 10 0 ppm

4.1.4 (2*R*,3*R*,4*R*)-3,4-Bis(benzyloxy)-2-((benzyloxy)methyl)-3,4-dihydro-2*H*-pyrrole 1-oxide (7)

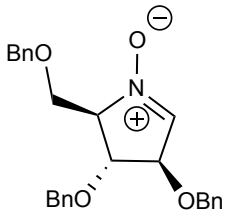

7

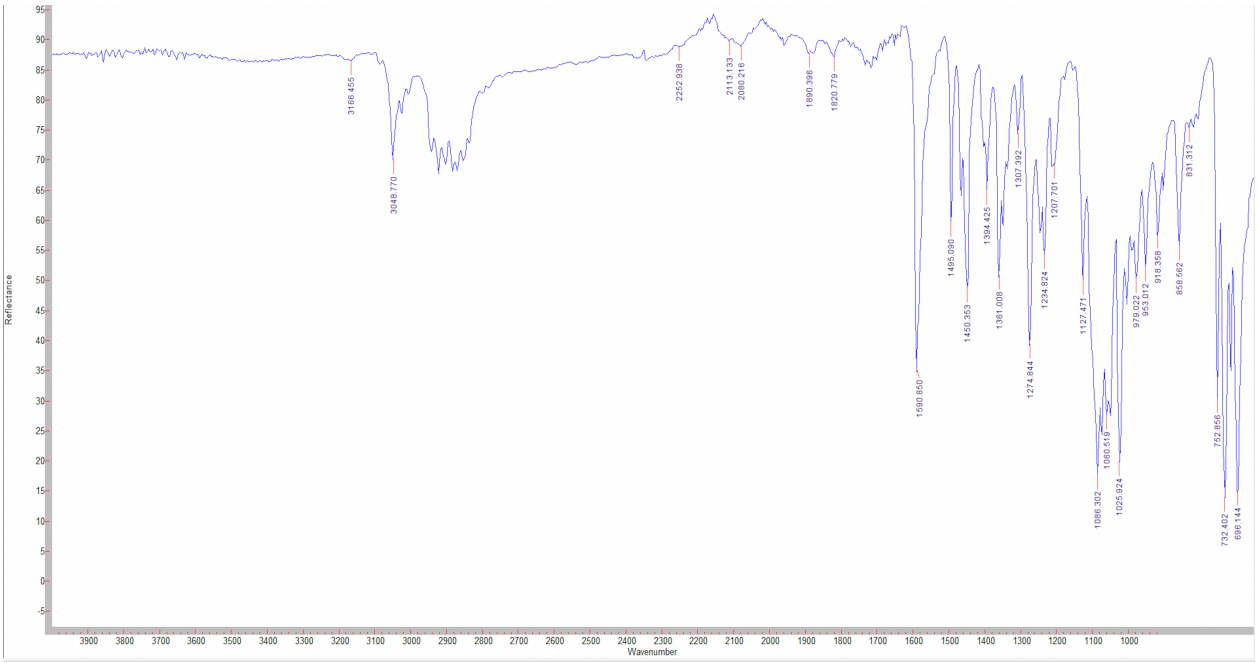

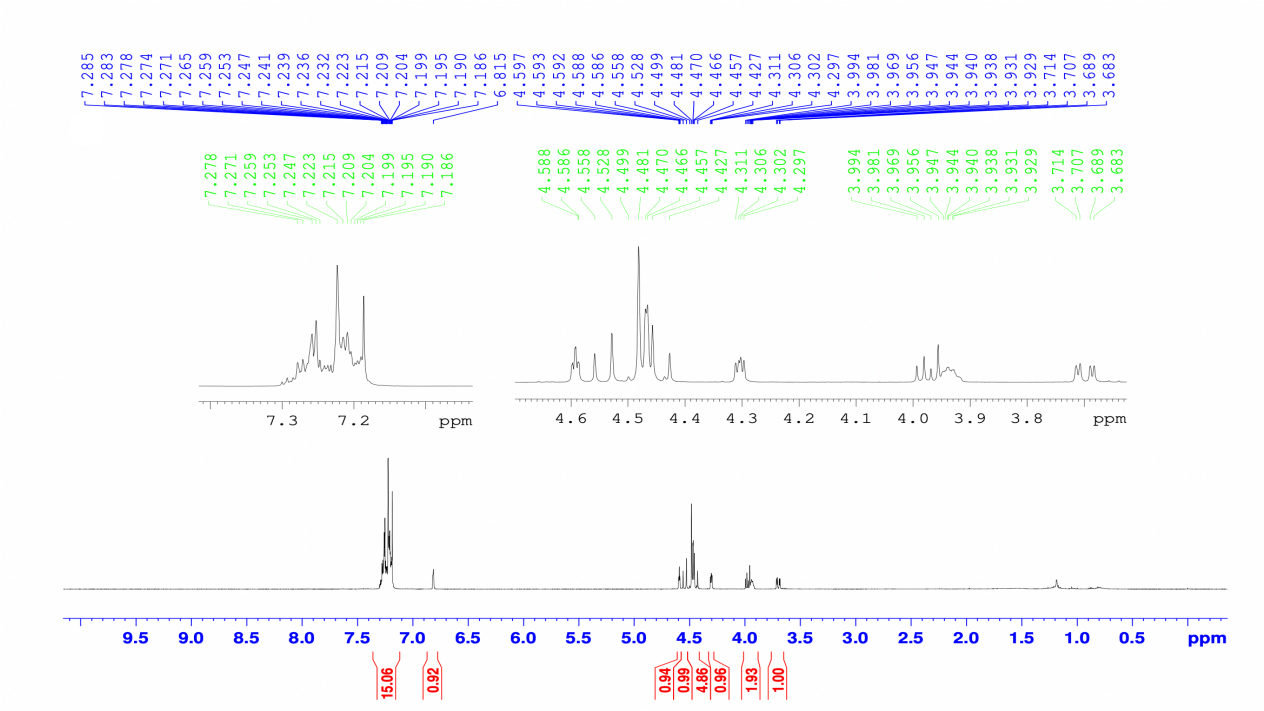

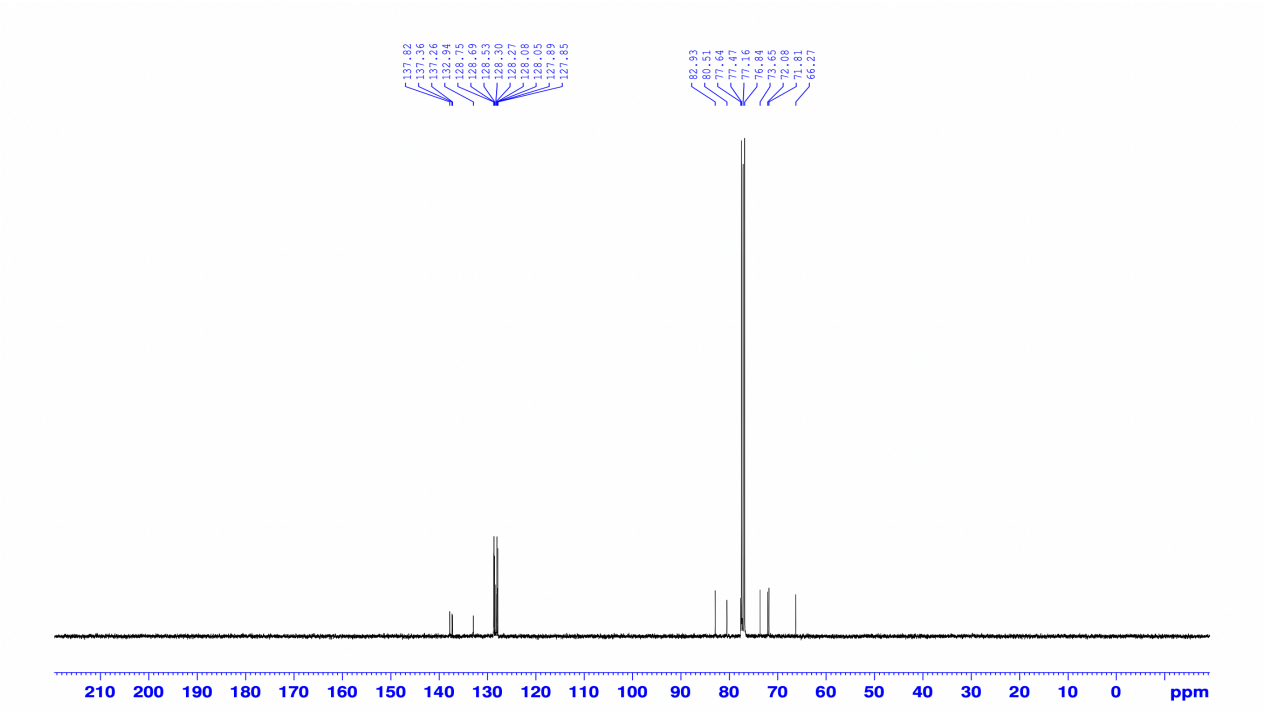
137.82
137.36
137.26
132.94
128.75
128.69
128.53
128.30
128.27
128.08
128.05
127.89
127.85
82.93
80.51
77.64
77.47
77.16
76.84
73.65
72.08
71.81
66.27
210 200 190 180 170 160 150 140 130 120 110 100 90 80 70 60 50 40 30 20 10 0 ppm

4.1.5 (2*R*,3*R*,4*R*)-3,4-Bis(benzyloxy)-2-((benzyloxy)methyl)pyrrolidine (9)

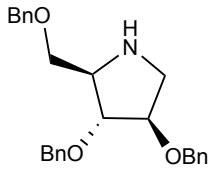

9

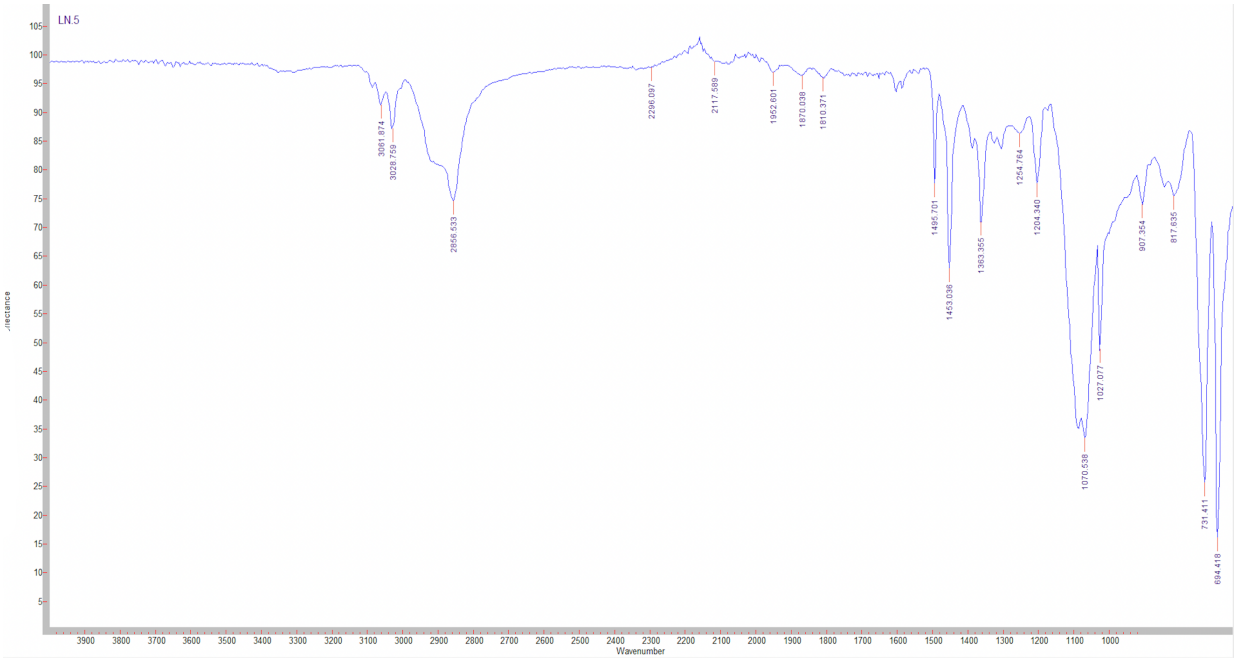

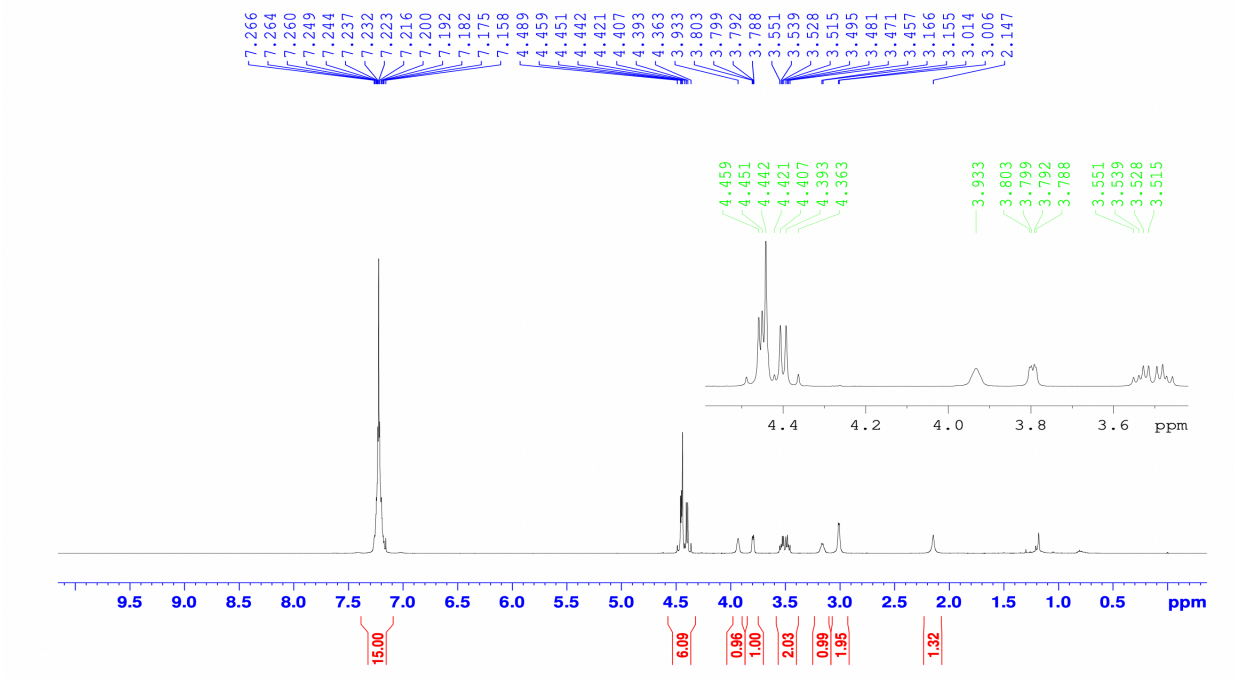

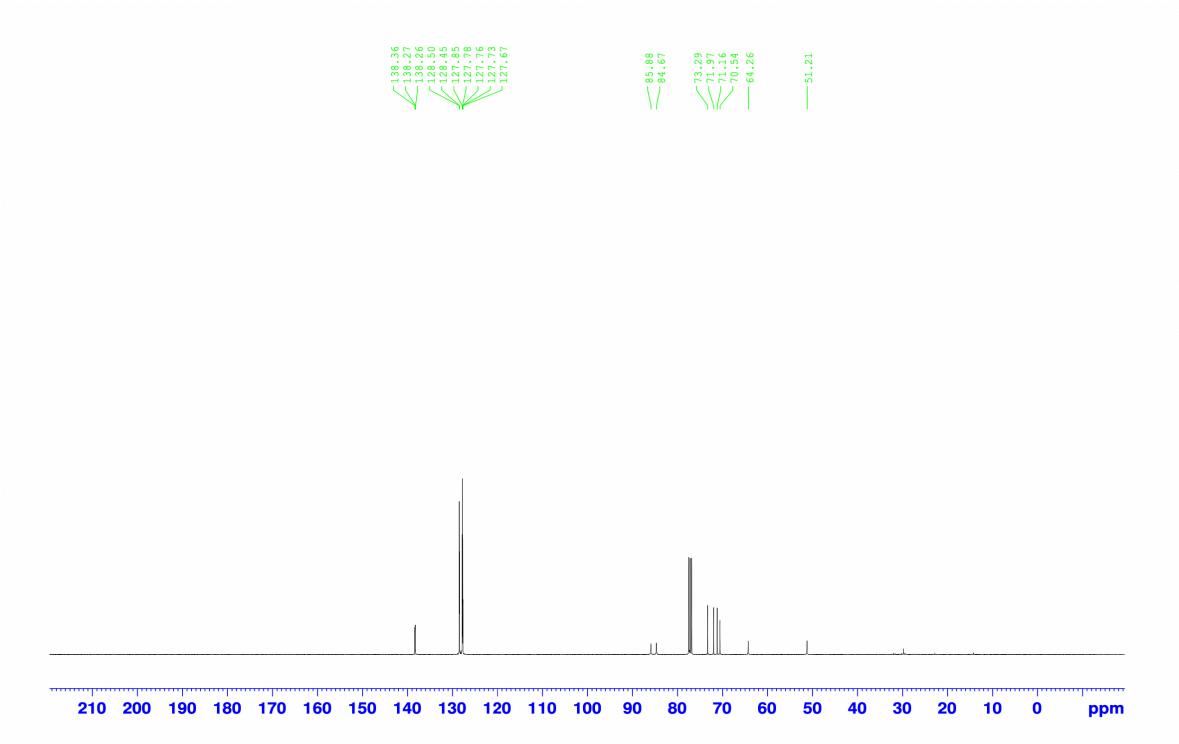
138.36
138.27
138.26
128.50
128.45
127.85
127.78
127.76
127.73
127.67
85.88
84.67
73.29
71.97
71.56
70.54
64.26
51.21
210 200 190 180 170 160 150 140 130 120 110 100 90 80 70 60 50 40 30 20 10 0 ppm

4.1.6 (1*R*,2*R*,3*R*) -2,3-Bis(benzyloxy)-1-((benzyloxy)methyl) -5-azaspiro[4.4]nonan-5-ium-bromide (10)

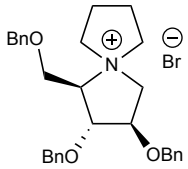

10

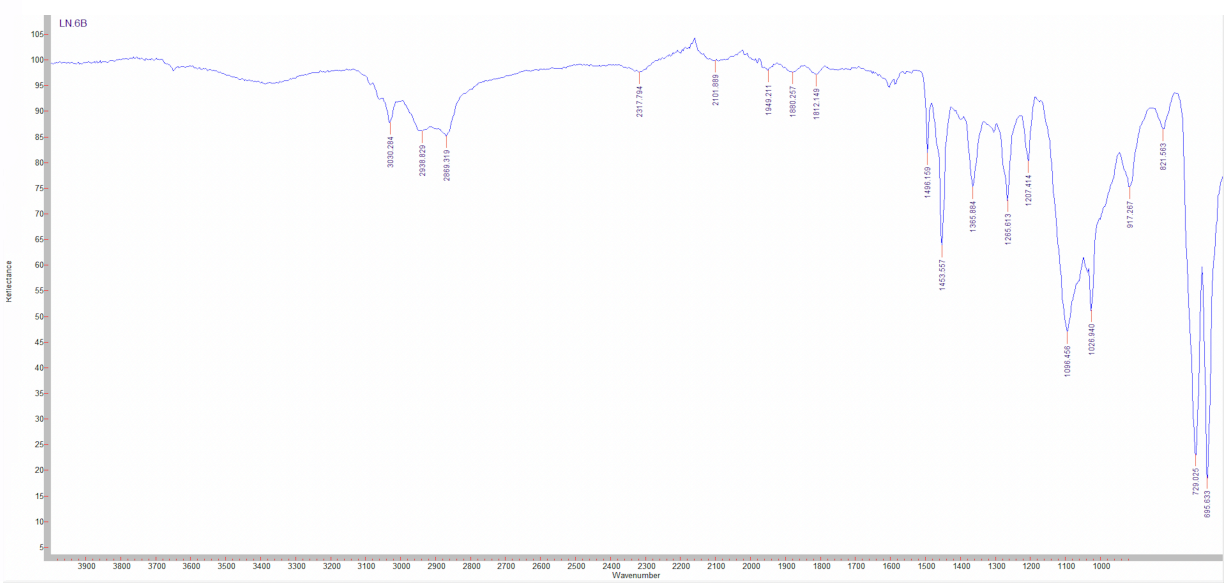

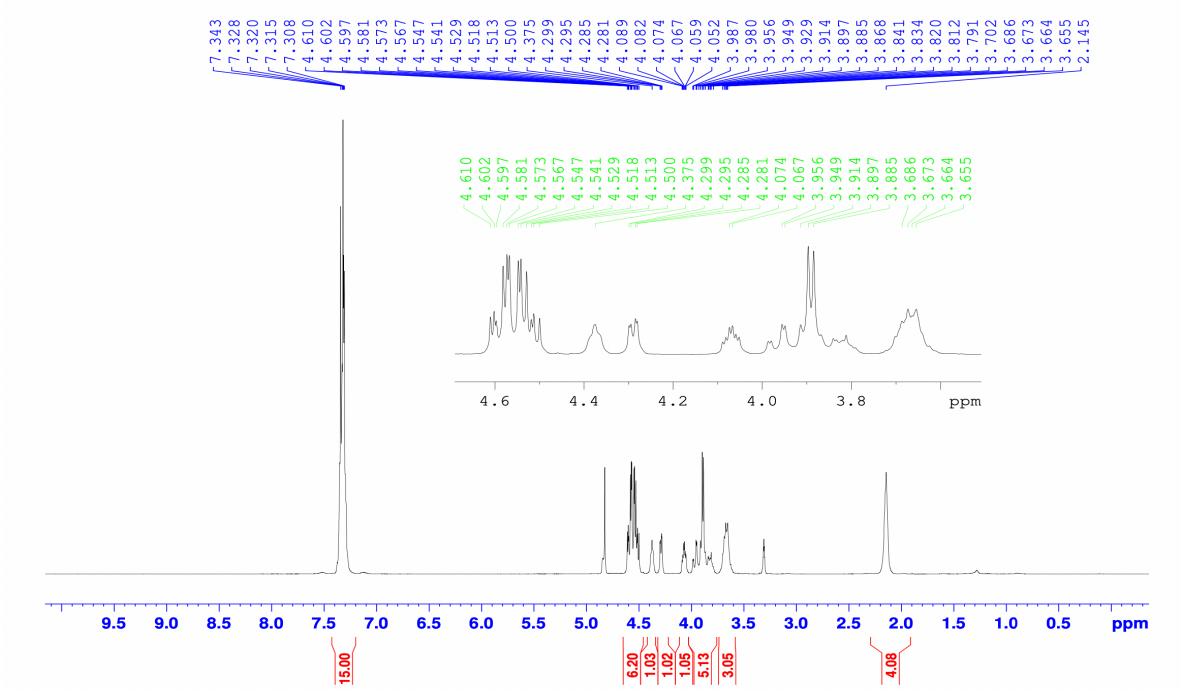

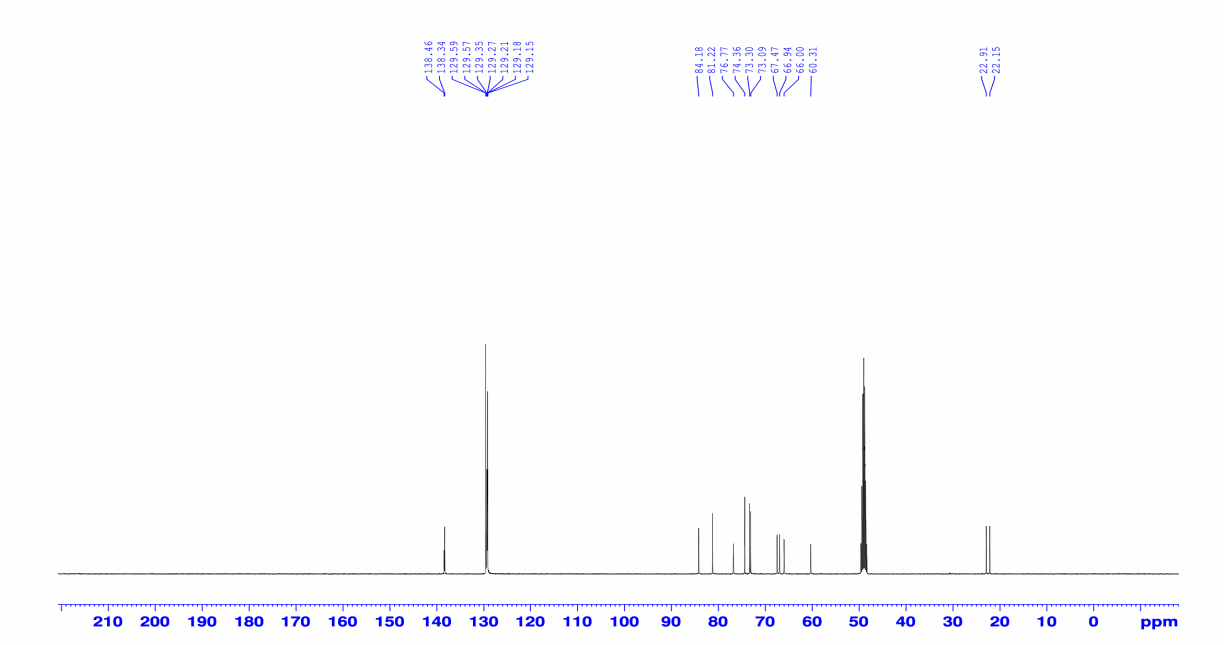
138.46
138.34
129.59
129.57
129.35
129.27
129.21
129.18
129.15
84.18
81.22
76.77
76.36
73.30
73.09
67.47
66.94
66.00
60.31
22.91
22.15
210 200 190 180 170 160 150 140 130 120 110 100 90 80 70 60 50 40 30 20 10 0 ppm

4.1.7 (1*R*,2*R*,3*R*)-2,3-Dihydroxy-1-(hydroxymethyl)-5-azaspiro[4.4]nonan-5-ium-bromide (11)

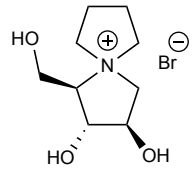

11

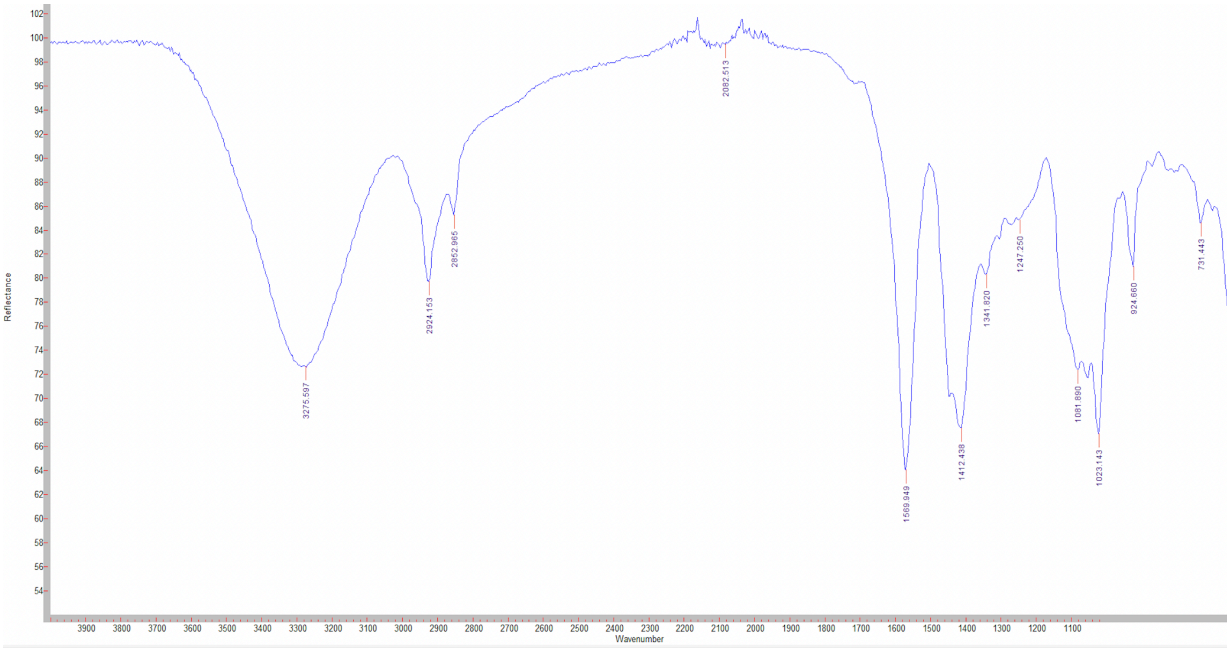

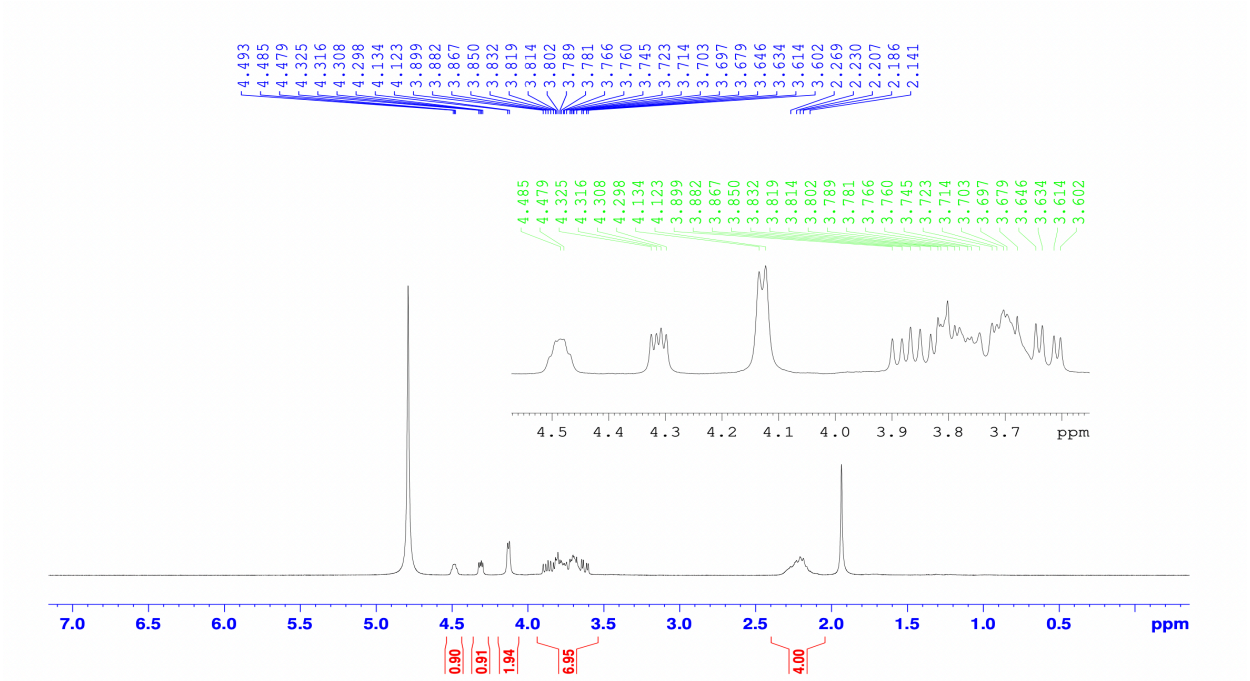

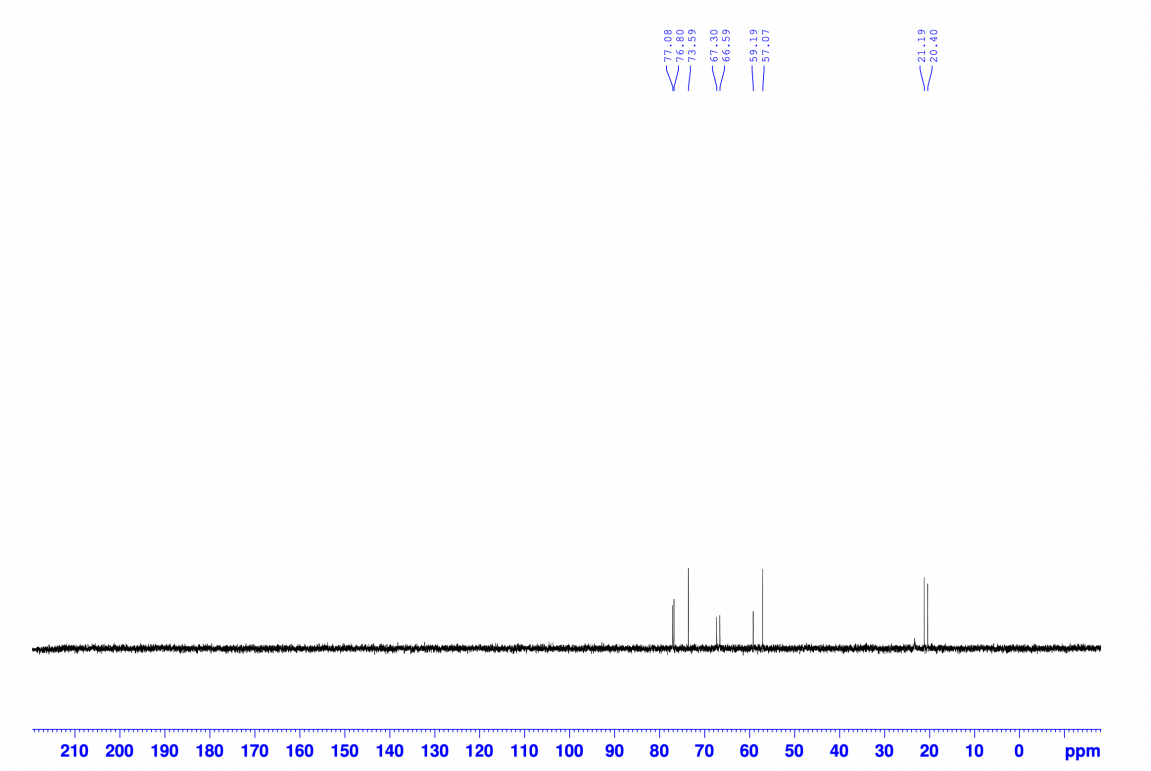
77.08
76.80
73.59
67.30
66.59
59.19
57.07
21.19
20.40
210 200 190 180 170 160 150 140 130 120 110 100 90 80 70 60 50 40 30 20 10 0 ppm